universität wien

MASTERARBEIT

Titel der Masterarbeit

"Monitoring techniques for studying mobility of iron oxide nanoparticles during field application"

verfasst von

Mag. Stefan Holzner

angestrebter akademischer Grad

Master of Science (MSc)

Wien, Juli 2015

Studienkennzahl lt. Studienblatt:	A 066 299
Studienrichtung lt. Studienblatt:	Interdisziplinäres Masterstudium Environmental Sciences
Betreut von:	Univ.-Prof. Dr. Thilo Hofmann

Abstract

The use of iron oxide nanoparticles (NPs) to enhance *in situ* biodegradation of a wide range of recalcitrant water contaminants is a promising technology. Aggregation, transport and deposition behavior of iron oxide NPs have already been reported in column experiments (Tosco et al., 2012), but further *in situ* implementation of iron oxide NPs requires detailed information on their mobility and particle tracking techniques.

This master thesis tested different methods to detect and characterize iron oxide NPs provided by the Helmholz Zentrum München (HMGU) via particle size, zeta potential, turbidity, total iron, and UV-absorption. After testing the methods in batch scale experiments on their suitability, the applicable techniques were further tested and adapted to detect the iron oxide particles during lab scale column experiments. The data from these experiments were then used and modeled to acquire transport parameters for the iron oxide NPs. The successfully tested methods were applied in a pilot scale container experiment at the Versuchseinrichtung zur Grundwasser- und Altlastensanierung (VEGAS, Stuttgart, Germany). For the container experiment a sampling plan had to be developed by combining the particles' transport parameters with information gained from a hydraulic model of the container.

Through the different steps of the experiments (batch scale and lab scale) it became evident, that only total iron (inductively coupled plasma optical emission spectrometry), turbidity (90° scatter method), and particle size measurements (dynamic light scattering) were applicable for detection of the iron oxide NPs in the pilot scale experiment. In addition to particle detection, turbidity measurements can be used to calculate the particle concentration.

The column experiments, performed with flow rates of 10.5 mL/min and 1.06 mL/min (corresponding to flow velocities of 100 m/d and 10 m/d) and NP suspensions with particle concentrations of 1 g/L and 10 g/L, showed that the iron oxide NPs are highly mobile with a recovery rate of 0.98. In experiments with high particle concentrations (10 g/L) and low flow rates (1.06 mL/min) particles got retained in the porous medium of the column, reducing the recovery rate down to a minimum of 0.72. Very similar results were delivered by modeling the breakthrough curves of the column experiments. The effect of ionic strength, pH, particle concentration, and flow rate on aggregation, size, sedimentation, zeta potential, and mobility of the particles could be seen in the results from the experiments.

The most promising methods for particle detection were applied in a pilot scale experiment, showing the effectivity, but also the limits of the measured parameters which are susceptible to errors. However, if the parameters are interpreted in concert, the errors can be identified and corrected.

The results of this thesis and the pilot scale experiment will be used in a designated field test, where the iron oxide NPs will be injected into a contaminated aquifer body in the Czech Republic.

Zusammenfassung

Die Verwendung von Eisenoxyd Nanopartikeln um den *in situ* Abbau von renitenten Wasserschadstoffen durch Bakterien zu fördern, ist eine vielversprechende Technologie. Aggregations-, Transport- und Ablagerungsverhalten von Eisenoxyd Nanopartikeln wurden bereits in Säulenexperimenten studiert (Tosco et al., 2012). Eine zukünftige tatsächliche Umsetzung dieser Eisenoxyd Nanopartikel Technologie benötigt jedoch weitere detaillierte Informationen bezüglich der Mobilität und Techniken um die Nanopartikel während der Anwendung nach zu weisen.

Deshalb wurden in dieser Masterarbeit verschiedene Methoden getestet, um Eisenoxyd Nanopartikel, welche vom Helmholz Zentrum München (HMGU) zur Verfügung gestellt wurden, anhand von Partikelgröße, Zeta Potential, Trübheit, Gesamteisen und UV-Absorption nachzuweisen. Diese Methoden wurden in Grundlagen-Experimenten auf ihre Eignung für die Partikel getestet. Anschließend wurden die geeigneten Methoden weiter geprüft, und für den Nachweis der Eisenoxyd Nanopartikel in Säulenversuchen angepasst. Des Weiteren wurden die Säulenversuche modelliert, um Transportparameter für die Nanopartikel zu erhalten. Am Ende wurden die erfolgreich getesteten Methoden in einem Pilotversuch, dem Containerexperiment in der Versuchseinrichtung zur Grundwasser- und Altlastensanierung (VEGAS, Stuttgart) angewendet. Für das Containerexperiment musste ein Probennahme-Plan erstellt werden, in welchem die Transport-Parameter der Nanopartikel mit Informationen einer hydraulischen Modellierung des Containers kombiniert wurden.

Über die verschiedenen Stufen der Experimente (Grundlagen- und Säulen-experimente) wurde herausgefunden, dass lediglich Partikelgrößen- (dynamische Lichtstreuung), Trübheits- (90° Streumethode) und Gesamteisenmessungen (optische Emissionsspektrometrie mittels induktiv gekoppelten Plasmas) für den Nachweis der Eisenoxyd Nanopartikel im Pilotversuch in Frage kommen. Die Trübheitsmessungen können, zusätzlich zum Partikelnachweis auch zur Berechnung der Partikelkonzentration der gemessenen Suspension herangezogen werden.

Die Säulenversuche, durchgeführt mit Fließraten von 10,5 ml/min und 1,06 ml/min (dies entspricht Fließgeschwindigkeiten von 100 m/d und 10 m/d) und NP Suspensionen mit Partikelkonzentrationen von 1 g/l und 10 g/l, ergaben mit Rückgewinnungsraten von 0,98, dass die Eisenoxyd Nanopartikel sehr mobil sind.

Lediglich in Experimenten mit hohen Partikelkonzentrationen (von 10 g/l) und geringen Fließraten (von 1,06 ml/min) wurden Partikel im porösen Medium der Säulen zurückgehalten, und die Rückgewinnungsraten wurden bis auf ein Minimum von 0,72 gesenkt. Sehr ähnliche Resultate lieferten die Modellierungen der Säulenexperimente. Des Weiteren wurden, zusätzlich zum Effekt der Fließrate auf die Partikelmobilität, Beweise für die Effekte von Ionenstärke, pH und Partikelkonzentration auf Aggregation, Partikelgröße, Ausfällung und Zeta Potential gefunden.

Im letzten Schritt wurden dann die geeignetsten Nachweismethoden für die Partikel im Pilotversuch angewendet. Dort zeigte sich die Effektivität der gemessenen Parameter, aber auch deren Grenzen und Bereiche, welche besonders für Fehler anfällig sind. Aber wenn die Parameter in Kombination interpretiert werden, können die Fehler erkannt und korrigiert werden.

Die Ergebnisse dieser Arbeit und des Pilotversuches werden in weiterfolgenden Feldversuchen, in welchen die Eisenoxyd Nanopartikel in einen kontaminierten Grundwasserkörper in der Tschechischen Republik injiziert werden sollen, eingesetzt werden.

Contents

List of figures

List of tables

1 Introduction

For sustaining life, water is one of the basic necessities. Global water utilization has doubled every 15 years, due to industrialization, urbanization, and population growth, leading to scarcity of water resources – thus creating challenges for over 40 % of the world population, as stated by the World Health Organization (WHO) (Fu et al., 2014). Further, the negligent way, how e.g. liquid wastes were and still are disposed (direct pumping into the ground, migrating into the ground from leaky storages or surface spills, etc.), leads to contamination of drinking water sources (O'Carroll et al., 2013), impairing the situation of water availability even more.

The awareness of the hazards of such contaminated sites and the subsequent pollution in the groundwater has been increasing over the last decades. The count of sites that have been recognized for the need to be remediated is increasing every year. Only in the European Union over three million contaminated sites were reported and remediation of at least 250000 sites is required (De Boer, 2012; Swartjes, 2011).

Two of the major remediation technologies are called adsorptive and reactive, and *in situ* and *ex situ*. Adsorptive technologies remove pollutants (particularly metals) via sequestration. On the other hand, reactive remediation technologies promote and sometimes enable the degradation of pollutants. *Ex situ* methods work by treating the polluted material after removing it to a better suited location, both on-site and off-site (e.g. pump and treat). *In situ* techniques on the other hand work by treatment of pollutants in the subsurface (e.g. permeable reactive barriers, which are trenches in the subsoil, filled with a reactive material, to intercept and react with the pollutant) (De Boer, 2012; Tosco et al., 2014; Tratnyek & Johnson, 2006).

Another remediation method, is the monitored natural recovery or monitored natural attenuation (MNA). It refers to letting natural processes take care of the pollutant in question. A wide range of biological, chemical, and physical processes are considered relevant for MNA (Geiger et al., 2009).

Most existing technologies are rarely able to achieve clean up goals on the contaminated sites. According to O'Carroll et al. (2013) the problem relates to the inability of the existing technologies to remove, sequester or convert sufficient pollutant mass to significantly diminish aqueous phase concentrations and pollutant flux.

In almost 20 years, the multidisciplinary nano "boom" has led to a broad spectrum of groundbreaking technologies; ranging from enhanced drug delivery systems to new remediation techniques for contaminated water. Especially in the field of groundwater remediation the global nano-revolution has triggered deep interest. As against conventional macro-scale materials, nanomaterials show considerable improvements in surface area to mass ratios, thereby conserving raw materials and energy, just by using a smaller amount of material to reach the same goal, and thus allowing substantial cost savings. The colloidal size of nanomaterials enables subsurface deployment by injection, leading to a faster treatment of the aqueous pollutants in terrestrial groundwater systems (Crane & Scott, 2012).

1.1 Use of nanoparticles for *in situ* remediation

Using nanoparticles (NPs) instead of larger particles for *in situ* remediation would give three advantages: (1) reaction rates of NPs are higher compared to larger particles (due to increased surface area where reactions can take place), (2) pollutants get degraded more completely by NPs than by larger particles (which do not react that easily with pollutants), and (3) NPs form more complete reacted byproducts from pollutants than larger particles (Geiger et al., 2009; Lowry & Johnson 2004; Nurmi et al., 2005; Shih & Tai, 2010). According to Geiger et al. (2009) some of this advantages are mainly due to the higher surface area to mass ratio, but also to the fact that NPs show different properties than the same material in its bulk form. Between 1 and 100 nm particles are in an intermediate state (between atomic and bulk state), where physical and chemical characteristics primarily rely upon the atoms at the surface than those in the interior of the bulk material (Akamatsu & Deki, 1997).

Numerous studies in the last 18 years have shown that nanometals are able to degrade a considerable variety of priority contaminants (trace elements, metalloids, and aromatic, polyaromatic and chlorinated organic compounds). Among this

nanometals tested for remediation purposes, nano iron or more precisely nanoscale zero valent iron (nZVI) is the most commonly studied (Braunschweig et al., 2013; O'Carroll et al., 2013). Responsible for reductive transformation or physical removal of pollutants by nZVI are corrosion reactions of the nZVI and its products (Crane & Scott, 2012).

1.2 Iron oxide nanoparticles

Not yet that commonly studied as nZVI, but none the less promising are iron oxides, e.g. the oxyhydroxide goethite with the formula α-FeO(OH). They have a considerable impact on the fate of organic pollutants by oxidative and reductive transformation processes. Through direct stimulation of microbial iron reduction by injecting iron oxide colloids into the subsurface, the contaminants can get degraded. That is because many microorganisms (e.g. *Geobacter sulfurreducens* [Bosch et al., 2010a; Bosch et al., 2010b]) can couple the reduction of iron oxides (using the iron oxide as an electron acceptor) to the oxidation of organic carbon and thereby metabolizing a wide range of recalcitrant water contaminants (e.g. BTEX), delivering a cost-effective *in situ* remediation technology (Braunschweig et al., 2013; Cundy et al., 2008; Tosco et al., 2012; Waychunas et al., 2005).

Since nanosized iron oxides are found abundantly in the environment, and the ability to reduce those iron oxides is common amongst microorganisms, this remediation technology could be classified as MNA (Cundy et al. 2008; Van der Zee et al., 2003; Weber et al., 2006). However, as iron oxide NPs are manufactured, modified, and, as previously mentioned, injected directly into the subsurface, boosting the microbial iron reduction, this method is considered as an *in situ* remediation technique.

Essential aspects of this *in situ* remediation technique are: the stability of the NPs regarding aggregation, their mobility in the aquifer body, their longevity under the prevailing subsurface conditions, and their reactivity with the target pollutants (O'Carroll et al., 2013; Tosco et al., 2014). To fulfill their purpose NPs should feature an ability to stay in suspension for as long as the slurry preparation, handling, and injection of the NPs into the aquifer body takes. Additionally they should possess an adequate mobility in the subsurface to allow a sufficing spread around the injection

well. Finally their reactivity should be persistent enough to cause a proper reduction/degradation of the target pollutant (O'Carroll et al., 2013; Tosco et al., 2014; Kanel et al., 2007).

1.2.1 Nanoparticle stability and mobility

Inorganic NPs (including iron oxide NPs) tend to agglomerate, which is shown by high sedimentation rates and their poor mobility in the environment (Grillo et al., 2015). The stability of the NPs can be increased via modifying their surfaces with compounds that are able to enhance the repulsion between them (Kango et al., 2013). Natural organic matter (NOM) can form a charged surface coating on NPs, which stabilizes them by electrostatic and steric interactions, and thus increases their mobility in the environment. For iron oxide NPs it has been shown that humic substances (HSs) can increase the particle stability (Baalousha, 2009; Grillo et al., 2015; Lowry et al., 2012). However, the mobility of the NPs is, once injected into a subsurface (porous medium), not only depending on the particle stability but also on particle-grain collisions (resulting in attachment/deposition) influenced by filtration mechanisms in the porous medium, which are: (1) Brownian or molecular diffusion, describing random movement of colloidal particles due to thermal effects, (2) convective fluid flow, picturing particles motion with water, and (3) gravitational effects, responsible for their vertical movement (Elliott & Zhang, 2001). Since the decisive mechanism is mainly depending on the particle size, and common aquifer pore diameters range from 200 nm (silty aquifer) to 0.1 mm (gravel aquifer), a NP size ranging from 100 to 200 nm is preferable. That way the NPs' mobility is improved, and simultaneously the retention in the subsurface based on physicochemical filtration is reduced (De Boer, 2012; Elimelech et al., 2000; O'Carroll et al., 2013). For that reason, the surface charge of colloids and porous medium, as well as the chemical composition of the pore water and its flow rate play an important role in the deposition and release (mobility in the subsurface) of iron-oxide NPs (Tosco et al., 2012).

1.2.2 Nanoparticle reactivity

Once the NPs reach the contaminant in the subsurface, the interest lies on their reactivity. The reactivity of iron oxides is defined by how they are capable to promote the microbial oxidation of the pollutant, and how fast they can accomplish such a promotion. Bosch et al. (2010b) found that nanosized iron oxide aggregates get reduced up to 30 times faster by microorganisms than macroaggregated iron oxides. They further observed a catalytic effect of the nanosized iron oxides upon the reduction of bulk iron oxides, advancing its reduction rates by 3 to 4 times. It is assumed that the nanosized iron oxide acts as an electron shuttle between the bulk iron oxide and the cell surface (Bosch et al., 2010b).

1.3 Nanoparticle injection

NP injection is basically possible in all terrestrial groundwater systems. In order to perform a successful remediation, the geologic and contaminant plume disparities must be determined together with a hydraulic and geochemical model. If done so, the right NP suspension composition, and deployment strategy can be chosen (Crane & Scott, 2012). In medium-coarse formations permeation injection can be used. With low injection rates and pressures, the particles get introduced into the subsurface via piezometers or gravity wells. In medium to low permeability formations direct-push, pneumatic or hydraulic fracturing are advised. Direct-push injections are performed by using a direct push apparatus (no predrilled borehole) to bring the particles into the contaminant plume (see Figure 1.1). Pneumatic (using a gas, e.g. air or nitrogen) or hydraulic (using an aqueous guar gel-sand-slurry) fracturing on the other hand create unpropped or sand-propped fractures in the formation, into which the NPs can subsequently be introduced. Direct-push, pneumatic, and hydraulic fractioning are all performed under the use of high pressures and flow rates (Christiansen et al., 2010; Tosco et al., 2014).

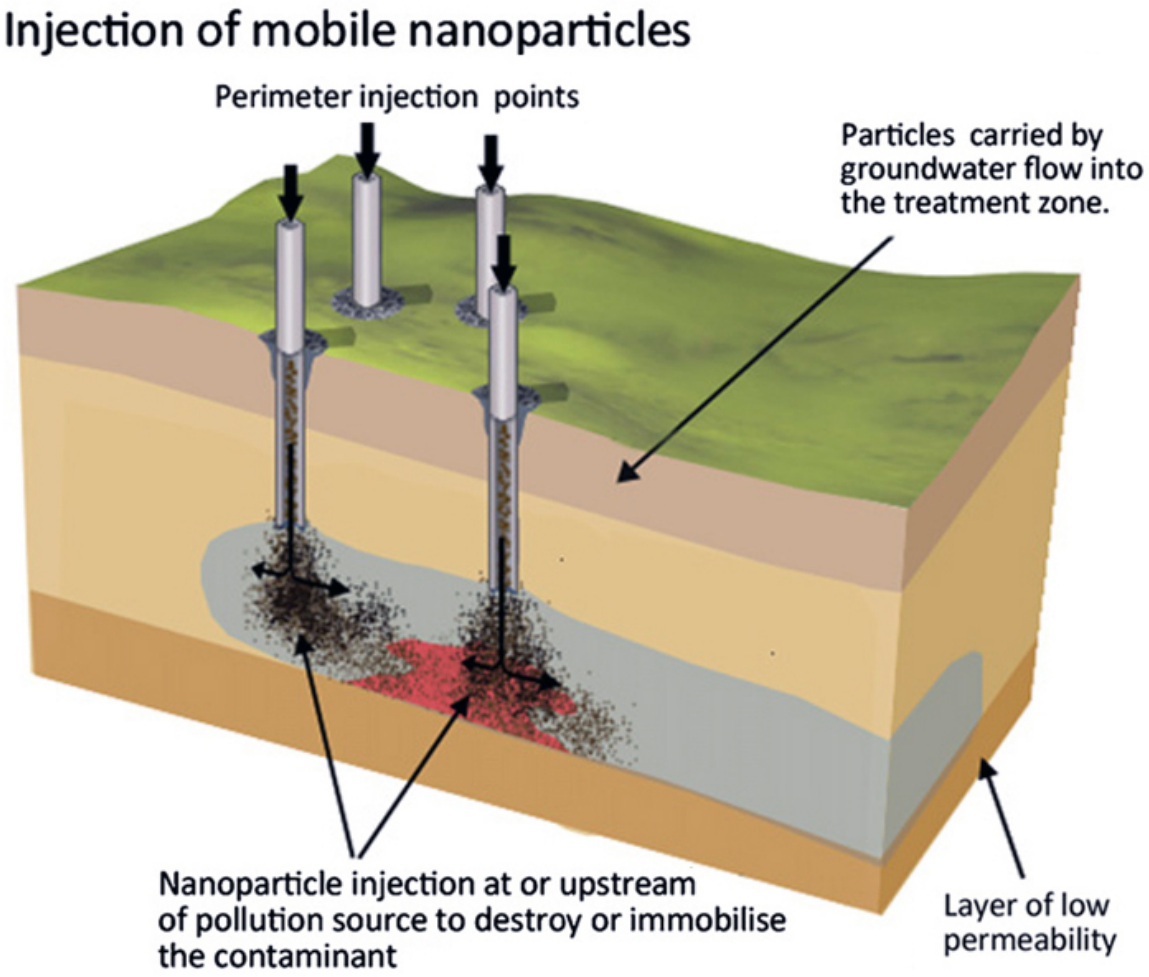

Figure 1.1: Sketch of an injection of mobile NPs into the subsurface to treat a contaminated aquifer body (based on Crane & Scott, 2012).

1.4 Nanoparticle detection

For a successful application of NPs for *in situ* remediation it is crucial to know, if the contaminants can get displaced by the injected fluid, and if the NPs reach the contaminant plume, stay in the reaction zone, or if they are further transported downstream (Bennett et al., 2010). For that reason, accurate methods to detect, identify, and quantify the NPs injected into the subsurface are needed (De Boer, 2012; O'Carroll et al., 2013). The transport of e.g. nZVI is usually monitored by the observation of alterations in the aqueous geochemistry caused by the NPs, like oxidation reduction potential (ORP), total iron, total solids, suspended solids, pH, and dissolved oxygen (Johnson et al., 2013). As these parameters do not differentiate

actual particles from dissolved corrosion species and geochemical changes, the NPs presence cannot be verified (O'Carroll et al., 2013).

Henn et al. (2006) used visual observation to detect nZVI, recognizing iron NPs. Already very low concentrations of iron stain a sample black, but further quantitative distinction is not possible (De Boer, 2012).

According to Simonet & Valcárcel (2009) there are several analytical methods which can be used to monitor NPs in the environment, but they still need to be improved regarding sensitivity and selectivity. Such techniques are (1) transmission electron microscopy (TEM), atomic force microscopy (AFM), and scanning electron microscopy (SEM) delivering images of the NPs, and (2) inductively coupled plasma optical emission spectroscopy (ICP-OES) and mass spectrometry (ICP-MS), providing an average bulk chemical composition of the sample (Simonet & Valcárcel, 2009). Lowry et al. (2012) have also stated that there are many instruments to measure NPs, however they are generally not capable to measure *in situ* or in environmentally relevant conditions, which would be preferable because of the instability of most NP dispersions in the environment (Simonet & Valcárcel, 2009).

On the other hand, De Boer (2012) developed a new technique, using the susceptibility (magnetization in a material to a corresponding magnetizing force) of iron, which enabled him to measure the nZVI concentration *in situ* and its change during the injection.

2 Research objectives

This master thesis was carried out in the course of the EU project: “Taking Nanotechnological Remediation Processes from Lab Scale to End User Applications for the Restoration of a Clean Environment” (NanoRem).

NanoRem, funded by the European Union 7th Framework Programme (FP7/2007-2013) under grant agreement number (FP7-309517) is a large scale project, conceived to last four years, which started in February 2013. The goal of the project is to advance nanotechnology to become feasible, economical, safe, and applicable for *in situ* remediation. NanoRem further aspires to develop an encompassing understanding of the risk benefit of nanotechnology for the environment, sustainability, market demand, and stakeholder perception (Bardos et al., 2014).

28 partners (private companies, research institutions, and universities) from 13 countries (Austria, Czech Republic, Denmark, Great Britain, Germany, France, Israel, Italy, Netherlands, Norway, Portugal, Spain, and Switzerland) are involved in the NanoRem project. The University of Vienna with the Department of Environmental Geosciences is working on mobility and fate of NPs within NanoRem.

The aim of this master thesis inside the framework of the NanoRem project is to find, adapt, and test techniques which enable detection and quantification of iron oxide NPs, more precisely goethite nanoparticles (GNPs), after *in situ* application (for more details (see Figure 2.1).

1. Different detection methods (employable for the GNPs, in the field, in a short time, for small sample volumes) were considered, tested, and if applicable, aligned to their intended use (batch scale).
2. Suitable methods where tested in column experiments, and further adjusted. In this step the GNPs were additionally tested for their mobility (lab scale).
3. A sampling campaign was planned and elaborated (from a groundwater flow model to the sampling plan) for a container experiment at the

Versuchseinrichtung zur Grundwasser- und Altlastensanierung (VEGAS) in Stuttgart (Germany). The container experiment and the incidental sampling campaign (October 2014) delivered satisfying results (pilot scale).

The complete data evaluation of the samples taken during the container experiment was not part of this master thesis. The results of this thesis will be further used in a designated field study in the Czech Republic, where GNPs are planned to be applied for induced toluene bioremediation.

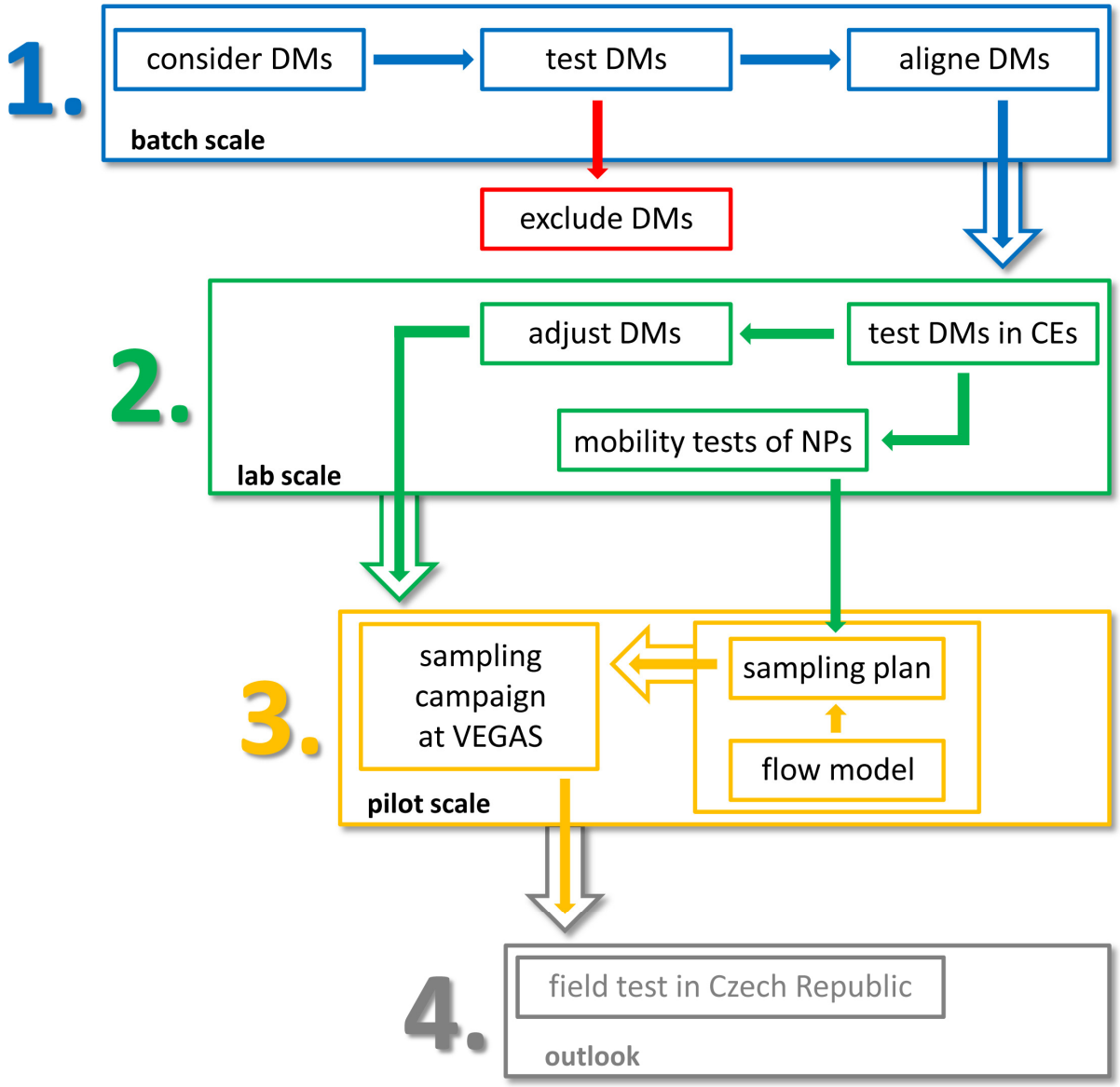

Figure 2.1: Flow chart of the approach of this master thesis: detection methods (DMs), column experiments (CEs), and nanoparticles (NPs).

3 Experimental

3.1 Materials

3.1.1 Nanoparticles and suspension preparation

The GNPs used in this thesis where produced and delivered by the NanoRem partner Helmholz Zentrum München (HMGU), German Research Center for Environmental Health (Institute of Groundwater Ecology). The NPs were delivered as a concentrated stock solutions in two batches (see 4.1.1 and 4.1.2). The first batch of goethite NPs (1st GNPs) contained, according to the manufacturer information: goethite particles (nano goethite, see Figure 3.1) with an organic coating (HSs), a mean hydrodynamic particle size (see 3.2.1.1) of 316 nm, and a zeta potential (see 3.2.1.2) of -56 mV; 5-10 g/L aluminum, and exhibited a pH of 9.4. The second batch of goethite NPs (2nd GNPs) were the further developed 1st GNPs and contained, also according to the manufacturer information: goethite particles (pristine nano goethite) with an organic coating (HSs), a mean hydrodynamic particle size of 215 nm, and a zeta potential of -54 mV; no aluminum, and displayed a pH of 9.2.

The 2nd GNPs where produced without aluminum because of the ecotoxicity of the aluminum towards bacteria (Chrzanowska & Załeska-Radziwiłł, 2014; Dong et al., 2014). In a field application, the ecotoxicity of the aluminum within the 1st GNPs suspension would have adverse effects on the bacteria, which the GNPs are supposed to promote to oxidize pollutants.

For GNP characterization, different particle concentrations were prepared depending on the characterization method.

For testing the detection methods and for compiling calibration curves nanoparticle suspensions with the following particle concentrations where prepared: 0.0005 g/L, 0.001 g/L, 0.005 g/L, 0.01 g/L, 0.05 g/L, 0.1 g/l, 0.5 g/L, 1 g/L, 1.5 g/L, and 2 g/L;

These suspensions were made by diluting the stock solution with Milli-Q water (Millipore, Elix®5-Milli-Q® Gradient A10) and F.I.m, a standard synthetic freshwater (see 3.1.2). The range of the concentrations was chosen to test the detection limits of the different methods. The GNP suspensions used in the column experiments had a particle concentration of 1 g/L, two additional experiments were carried out with a 10 g/L suspension (only for the 2nd GNP), the same concentration which was later used in the container experiment (see 3.2.4). The GNP suspensions for the column experiments were all prepared with F.I.m.

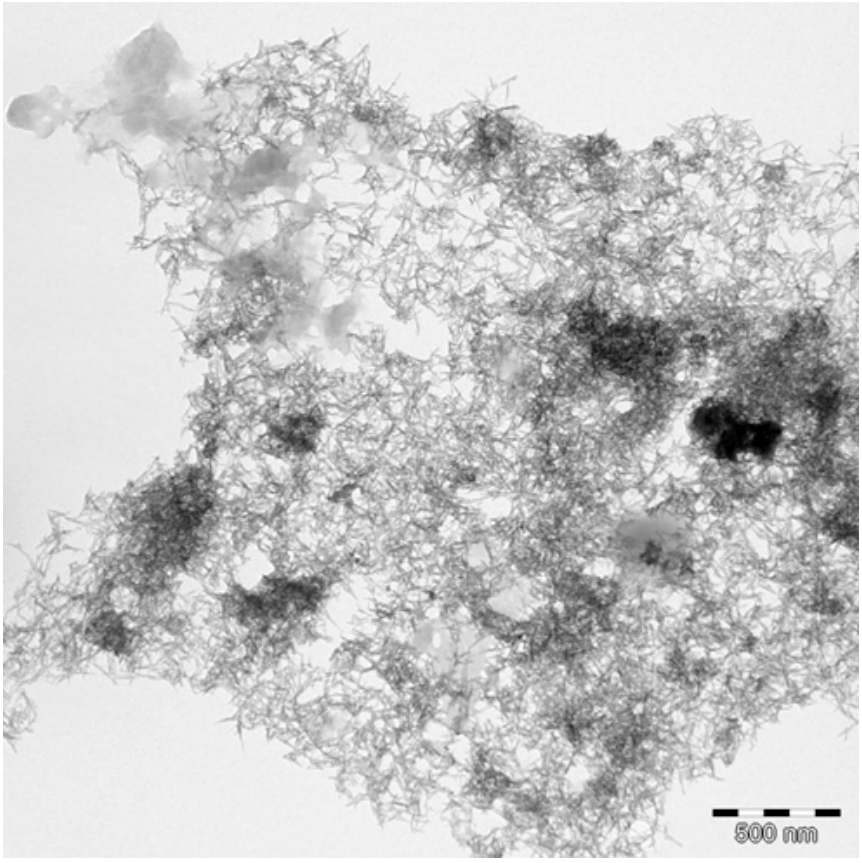

Figure 3.1: TEM image of uncoated GNPs (provided by HMGU).

3.1.2 Porous medium and standard synthetic freshwater

The porous medium for the column experiments was the same sand as in the pilot scale experiment. Since in the pilot scale experiment two different types of sand (medium sand and coarse sand) were to be used, the medium sand (M.II)[1], in which the injection of the GNPs would take place, was chosen for the column experiments.

The M.II was provided by VEGAS, and a sieving analysis and a chemical analysis (elementary and X-ray Diffraction) was conducted for chemical composition and grain size distribution. Composition and characteristics of M.II are shown in Table 3.1 and Table 3.2.

Table 3.1: Chemical composition of the medium sand M.II

Chemical composition of M.II			
SiO_2 [%]	84.2	**Ba [mg/kg]**	318
Al_2O_3 [%]	5.69	**Cr [mg/kg]**	101
Fe_2O_3 [%]	0.85	**Ni [mg/kg]**	10
CaO [%]	2.27	**Sr [mg/kg]**	104
MgO [%]	0.26	**V [mg/kg]**	12
Na_2O [%]	1.01	**Zn [mg/kg]**	12
K_2O [%]	2.49	**Co [mg/kg]**	2
MnO [%]	0.02	**Cu [mg/kg]**	6
TiO_2 [%]	0.09	**Li [mg/kg]**	31
P_2O_5 [%]	0.05	**Pb [mg/kg]**	16
LOI [%]	2.22		

[1]According to the NanoRem standardized experimental protocols for mobility, reactivity and ecotoxicity studies, M.II is defined as a commercial available quartz material, which is required to be used for column and large scale experiments.

Table 3.2: Characteristics of the medium sand M.II

Characteristics of M.II	
Porosity	0.35
Bulk density [g/cm^3]	1.74
Surface charge [mV]	-39 ±7
Grain size distribution:	
d_{10} [mm]	0.23
d_{50} [mm]	0.63
d_{60} [mm]	0.9
d_{90} [mm]	3.3

All experiments were performed using a standard synthetic freshwater (F.I.)[2]. The F.I.m was chosen from three standard synthetic freshwaters with different hardness: soft (F.I.s), moderately hard (F.I.m), and very hard (F.I.h). It was chosen because of its similarity to the water being used in the pilot scale experiment, regarding ionic strength. The F.I.m was prepared following the modified protocol for standard synthetic freshwater (see Table 3.3), as described by US EPA (2002).

Table 3.3: Preparation of standard synthetic freshwater using reagent grade chemicals and Milli-Q water (based on US EPA, 2002).

	Reagent added [mg/L]				Approximate final water quality		
	$NaHCO_3$	**$CaSO_4 \cdot 2H_2O$**	**MgSO4**	**KCl**	**pH**	**Hardness***	**Alkalinity***
F.I.s	48.0	30.0	30.0	2.0	7.2-7.6	40-48	30-35
F.I.m	96.0	60.0	60.0	4.0	7.4-7.8	80-100	57-64
F.I.h	384.0	240.0	240.0	16.0	8.0-8.4	280-320	225-245

[2]According to the NanoRem standardized experimental protocols for mobility, reactivity and ecotoxicity studies, standard synthetic freshwater (EPA-821-R-02-012) is required to be used for laboratory scale experiments.

3.2 Experimental design

Concurrent with the aim of this thesis, segmented into three steps (see 2 and Figure 2.1), the experimental setup followed this structure:

1. In batch scale experiments different instrumental methods were tested with the 1st and 2nd GNP suspensions, and adapted to detect and characterize them.
2. In lab scale experiments 1st and 2nd GNP suspensions were pumped, following a protocol, through a porous medium, simulating field applications under controlled conditions. The methods, tested and adapted in the batch scale experiments, were then used to detect the particles in the outflow of the columns. Further, the gathered data was analyzed and modeled, to get mobility parameters for the tested GNPs.
3. In the pilot scale experiment at VEGAS the methods, acquired and adapted in batch and lab scale experiments, were used to detect the GNPs in the container after injection, and to map their movement within it. For the measuring campaign to be successful, a groundwater flow model (hydraulic model) of the container was made. In combination with the mobility parameters of the GNPs a reasonable sampling plan was developed.

3.2.1 Methods for iron oxide NP characterization and detection - batch scale

To detect the GNPs after injection, different methods to characterize, and thereby also to detect the NPs where taken under consideration and tested.

GNPs properties used for NP characterization were: (1) size, (2) surface charge, and (3) concentration. Parameters for those three properties are:

(1) Particle size,

(2) Zeta potential,

(3) Turbidity, total iron, and UV-absorption;

To determine those parameters there are various measurement principles and instruments which were used (see Table 3.4):

For the batch scale experiments, 1st and 2nd GNP suspensions were prepared from the stock solutions as described in 3.1.1. The following methods were tested in batch scale experiments for their applicability and suitability to detect the GNPs.

Table 3.4: Particle properties, their parameters, the measurement principle, and the instruments used to measure them.

Property	Parameter	Measurement principle	Instrument
Size	Particle size	Laser diffraction	Mastersizer
		Dynamic light scattering	Zetasizer
		Laser obscuration time	EyeTech
Surface charge	Zeta potential	Electrophoretic light scattering	Zetasizer
Concentration	Turbidity	90° scatter method	Turbidity meter
	Total iron	Inductively coupled plasma optical emission spectrometry	ICP-OES
	UV-absorption	Ultraviolet-visible spectrophotometry	UV-Vis

3.2.1.1 Particle size

To measure the particle size (diameter) of the GNPs in the different suspensions the following measuring principles and instruments were tested for their suitability:

In **laser diffraction** a laser beam, passing through the sample (dispersed particles), gets scattered (diffracted) by the particles, creating a specific scattering pattern. From the resulting scattered light pattern the particle size is calculated, applying the Mie theory. This technique is applicable for particles in the range from 0.02 µm to 2000 µm and delivers the particle size as volume equivalent sphere diameter. The instrument used, deploying laser diffraction, was the Mastersizer 2000 (Malvern Instruments, UK).

Dynamic light scattering (DLS) sometimes also referred to as Quasi-Elastic Light Scattering is a very fast method to measure particle size and particle size distribution. In DLS the Brownian motion of particles in a suspension scatters a laser light at different intensities, leading to the velocity of the Brownian motion. Applying the Stokes-Einstein relationship on this velocity yields the particle size as intensity averaged particle diameter. DLS can be used to measure particles between 0.3 nm and 10 µm (Kato et al., 2012). DLS does not gather the actual size (diameter) of particles, but the hydrodynamic diameter. The hydrodynamic diameter refers to how a particle diffuses within a fluid. Therefore the diameter obtained by DLS is that of a sphere with the identical translational diffusion coefficient as the particle. The Zetasizer Nano ZS (Malvern Instruments, UK) was the instrument of choice for DLS measurements. The samples were measured each ones with three runs in low volume disposable sizing cuvettes (ZEN0112). Samples with high particle concentrations (10 g/L) where diluted 1:10 with Milli-Q water before measurement. The distribution analysis of the samples was done with the general purpose (normal resolution) method of the Malvern Zetasizer software (v703-PSS0012-34-EN-JP).

In the **laser obscuration time** method laser light with a fixed velocity passes through a sample (dispersed particles), where it interacts with particles getting in its path. The time of obscuration measured by a detector is directly related to the particle diameters, and gets presented in number and volume distributions. This method is suitable for partilcles from 0.1 µm to 3600 µm. The GNPs characterisations by laser obscuration time where conducted with the EyeTech™ (Ankersmid, NL) instrument.

3.2.1.2 Zeta potential

In particle suspensions the surface charge determines the electrostatic interaction between the particles, and is crucial in understanding particle stability (see 1.2.1). The zeta potential is the key parameter describing the surface charge of particles in suspensions. Particles dispersed in aqueous media feature an electric charge, which is affecting the distribution of ions in the vicinity, forming an electrical double layer close to their surface. This double layer is subdivided into the so called stern layer (inner layer with strongly bound ions) and diffuse layer (outer layer with ions not that strongly bound). The zeta potential is the potential at a hypothetical plane (slipping plane) within the diffuse layer. It divides ions that move with a particle from ions which stay with the aqueous medium (see Figure 3.2). Such a movement can be induced e.g. by electrophoresis (Delgado et al., 2005; Kaszuba et al., 2010).

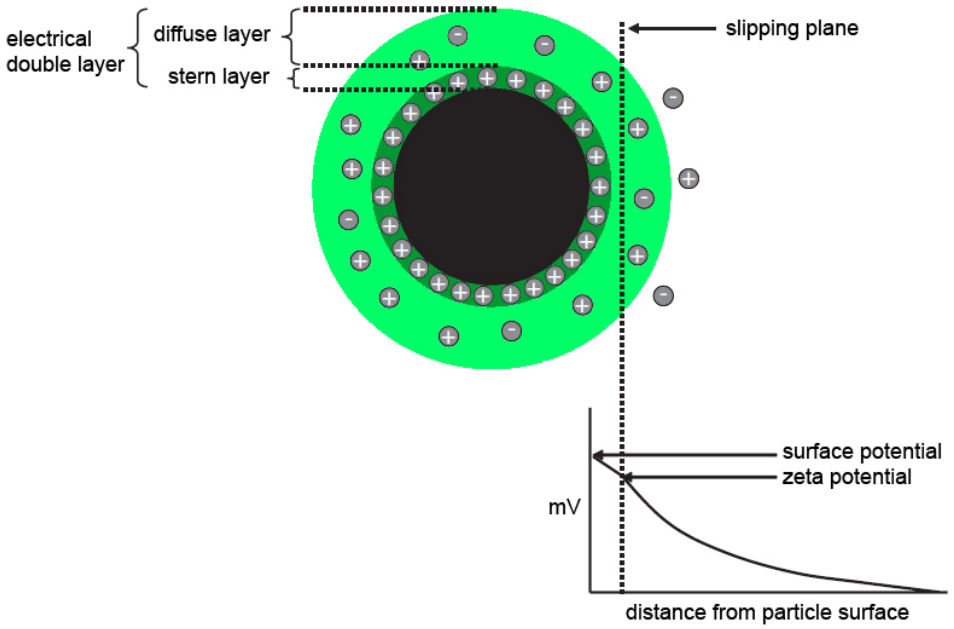

Figure 3.2: Sketch of the electrical double layer surrounding a particle in an aqueous medium and the position of the slipping plane, its electrical potential corresponds to the zeta potential (based on Kaszuba et al., 2010).

With **electrophoretic light scattering** (ELS) the electrophoretic mobility of dispersed particles is determined by applying an electrical field to the sample, which will induce the particles to migrate. The migration velocity (electrophoretic mobility) of

the particles is measured via the laser Doppler velocimetry method, based on the evaluation of the intensity autocorrelation function of the scattered light, and is related to their zeta potential (Delgado et al., 2005).

The zeta potential of the GNPs was determined with the Zetasizer Nano ZS (Malvern Instruments, UK). Also for this method, samples with high particle concentrations (10 g/L) where diluted 1:10 with Milli-Q water before measurement. The samples where measured with the measurement duration set on automatic (min. 10 and max. 25 runs) in clear disposable folded capillary zeta cells (DTS1060C). The general purpose analysis model of the Malvern Zetasizer software was used for data analysis.

3.2.1.3 Turbidity

Turbidity describes the haziness of a liquid. It is dependent on the amount of materials suspended in it, and their ability to decrease the passage of light through the liquid by absorbing or scattering the light. This parameter was used to determine the GNP concentration in the samples after directly connecting the turbidity of the suspension to its particle concentration (calibration curve, see Figure 3.3).

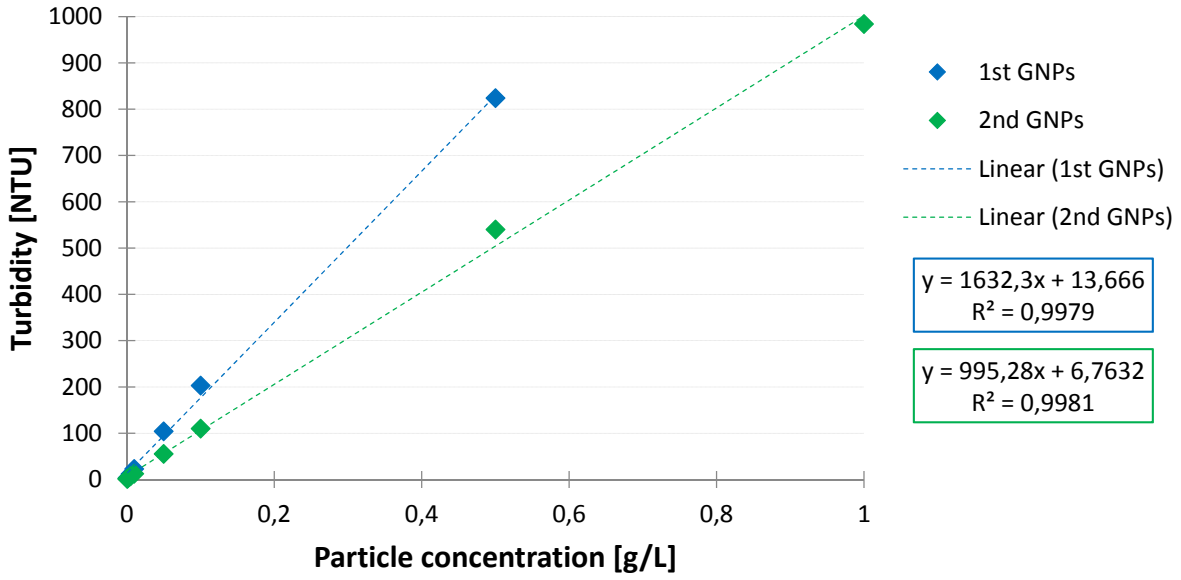

Figure 3.3: Turbidity of the 1st and 2nd GNP suspensions against their particle concentration.

The **90° scatter method**, applied in turbidity meters or nephelometers, is according to US EPA (2006) the most accurate method to measure turbidity. In this method, light emitted from a diode (LED with a wavelength of 860 ±30 nm, ISO 7027) or a tungsten lamp (with a color temperature of 2200 - 3000 K, EPA Method 180.1) shines through the sample where it gets scattered by particles. At a 90° angle to the incident light beam a photoelectric cell measures the intensity of the scattered light, correlating that signal to Formazin Nephelometric Units (FNU, ISO 7027) or Nephelometric Turbidity Units (NTU, EPA Method 180.1), both measures for turbidity. The turbidity was determined with the turbidity meter 2100N IS (Hach Lange, DE). The samples were measured in round glass cuvettes (LCW906) fitting the adapter for the turbidity meter after calibrating the instrument with Formazin standards (diluted from the Formazin Turbidity Standard 4000 NTU). Samples were diluted with Milli-Q water if the particle concentration was too high (measurement range from 0 to 1000 NTU).

3.2.1.4 Total iron

Total iron, referring to the overall concentration of iron, no matter its oxidation state in a sample, was measured. Like turbidity it was directly associated to the GNPs concentration in the particle suspension (calibration curve, see Figure 3.4). To measure the total iron, the samples needed to undergo pretreatment before being analyzed. The samples had to be diluted with Milli-Q water and digested by addition of HCl (30%) and HNO_3 (5 M).

Inductively coupled plasma optical emission spectrometry (ICP-OES) is used for quantitative and qualitative analysis of solid, fluid, and gaseous samples, by interpreting the electromagnetic radiation (characteristic for each chemical element) emitted from the excited atoms of the sample (OES). The excitation of the atoms is induced by inductively coupled plasma (ICP), a ca. 10000 K hot argon-plasma. To measure the samples for total iron, the ICP-OES Optima 5300DV (PerkinElmer, USA) was used.

Additionally the total iron and turbidity values, both directly linked to the particle concentration, were correlated with each other. This was done, to have an indicator of

how well the two different parameters match and if not, to see where the differences lie.

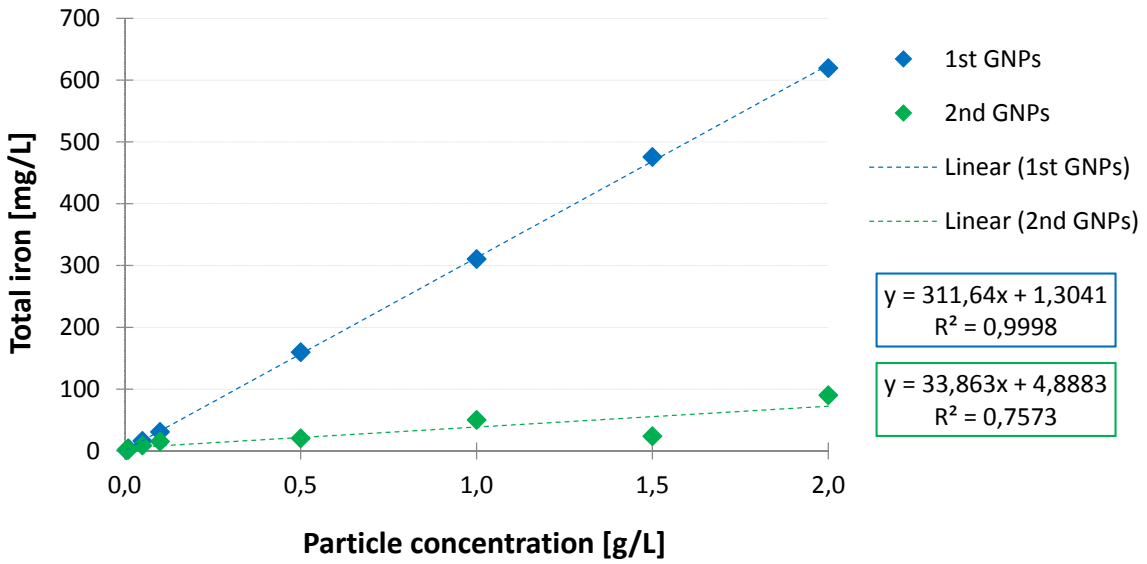

Figure 3.4: Total iron concentration of the 1st and 2nd GNP suspensions against their particle concentration. The difference between 1st and 2nd GNPs is probably caused by differences in production (see 4.2.2).

3.2.1.5 UV/VIS-absorption

In principle UV/VIS absorption is a process, where ultraviolet or visible light, in a wavelength range from 190 nm to 900 nm, gets absorbed by materials. This materials, e.g. iron oxides have specific absorption bands which can be attributed to different types of electronic transitions. Using the second derivation of the spectrum, goethite is identifiable at 480 nm (Szalai et al., 2013).

In **UV/VIS spectrophotometry** electromagnetic radiation over the whole UV/VIS light range scans both the sample cell and a reference cell. The transmitted radiation gets detected by a photocell, and the absorption gets recorded by a spectrometer via comparing the intensities of the radiation passing through the sample and the reference cell. The Lambda 35 UV/VIS spectrometer (PerkinElmer, USA) was used to measure the UV/VIS absorption of the samples.

3.2.1.6 Other relevant parameters

Sedimentation rate

The sedimentation rate indicates the tendency from particles in suspension to settle out of the fluid according to Stokes' law. It can be measured via multiple light scattering (MLS).

In **multiple light scattering** light from a near infrared (NIR) light source (880 nm) enters the sample, where it gets scatter by the particles in suspension. The intensity of the light leaving the sample gets measured by two detectors: (1) transmitted light in 0° from the light source, and (2) backscattered light in 135° from the light source; and is recorded in relation to the sample height. In that way phase separation (sedimentation) can be detected, and over time the sedimentation rate is derived. The sedimentation rate of the samples was measured with the Turbiscan™ Lab (Formulaction, FR).

pH

The pH is the negative logarithm of the hydrogen ion activity in an aqueous solution, and was measured using a pH meter with a pre-calibrated micro combination electrode (WTW, DE).

Electrical conductivity

The electrical conductivity is a measure for the ability of a material or fluid to conduct an electrical current. The GNP suspension's electrical conductivity was measured using a standard conductivity cell (Tetracon®325, WTW, DE).

3.2.2 Detection of iron oxide NPs in column experiments - lab scale

The lab scale experiments were designed to test the suitable detection methods on GNP suspensions after passing through a porous medium, and to detect and quantify filtration effects on the GNP suspensions. For this purpose column experiments were the best fit. Additionally they allowed to draw inferences about the GNPs mobility parameters. The experimental setup shown in Figure 3.5 was used for all column experiments. It was composed of a peristaltic pump (Ismatec®, DE), pumping GNP suspensions, kept in an ultrasonic bath (Sonorex RK 106, Bandelin electronic, DE), to reduce particle aggregation, through polytetrafluoroethylene (PTFE) tubing[3] into a borosilicate glass column (25 mm i.d., 220 mm length; Omnifit®, DE) packed with M.II. To ensure homogeneous distribution of the GNP suspension throughout the column, and to prevent the buildup of preferential flow paths, the suspension was pumped from bottom to top trough the column (Lewis and Sjöstrom, 2010). In the end, the effluent of the column was sampled by an Omnicoll auto-sampler (Lambda Instruments, CH) into vials. At both ends of the column pressure probes were connected to the tubes, to register any pressure differences between inflow and outflow, being an indicator for clogging phenomena (Hosseini & Tosco, 2013; Tosco & Sethi, 2010). The pressure probes were connected to a pressure meter HD2124.2 (Delta Ohm, IT) to record the pressure data. Each column experiment was carried out in duplicates simultaneously, with the same setup.

[3] PTFE, PVC or Butyl rubber tubing material is recommended to be used, according to the NanoRem standardized experimental protocols for mobility, reactivity and ecotoxicity studies.

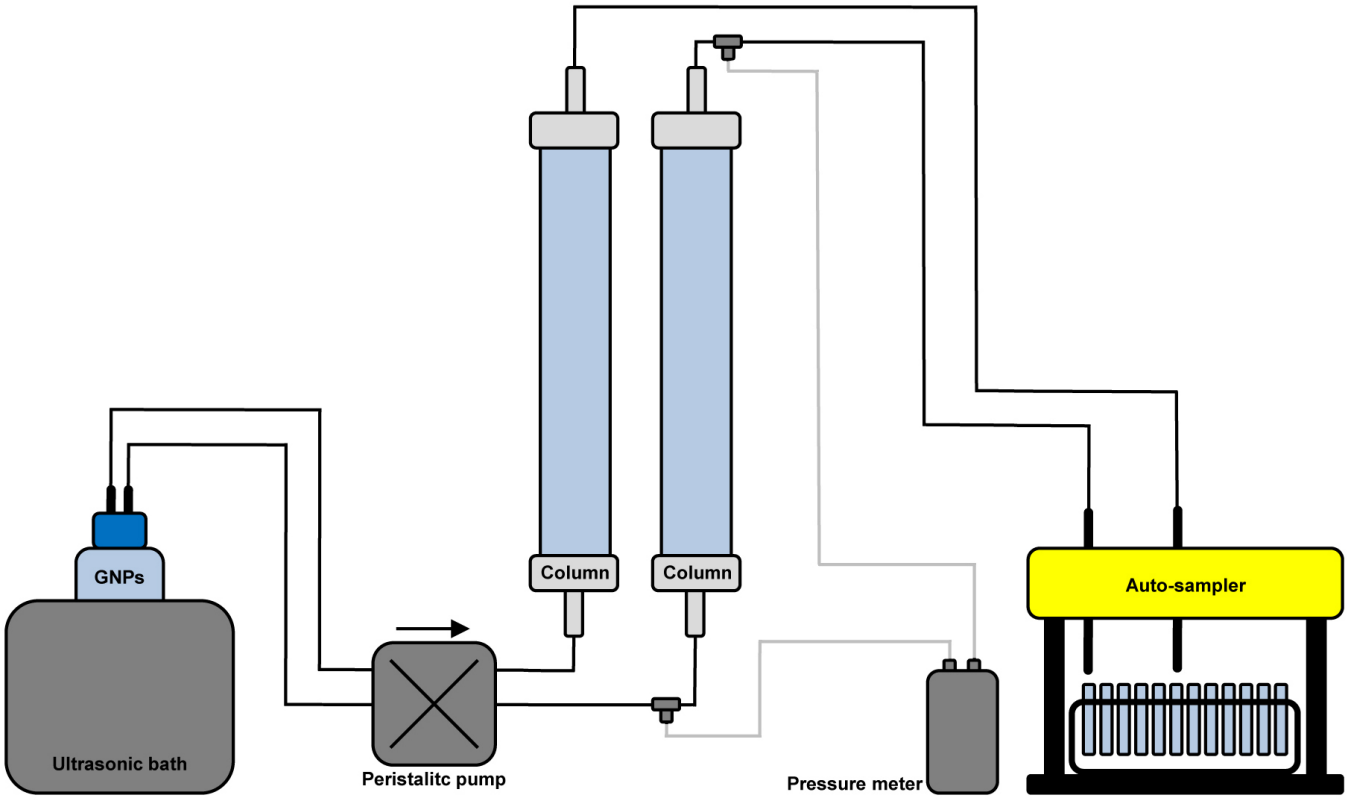

Figure 3.5: Sketch of the experimental setup of the column experiments.

Before packing, the inlet and outlet of the columns were equipped with nylon filters (hydrophilic, 180 µm, 25 mm, NY8H02500, EMD Millipore®) to prevent washout of the porous medium. Each column was then wet packed up to 20 cm with previously washed M.II and flushed with at least 5 pore volumes (V_P) to remove background turbidity (all with Milli-Q water). The tubing volume (V_T) was determined to later calculate the effective porosity (n_e) of the M.II in each column (equation (3.2) and (3.1)).

Each column experiment consisted of four different parts: (1) tracer experiment, (2) GNP injection, (3) flushing (all carried out with the same steady flow rate), and (4) column dismantle.

1. The tracer experiment was conducted to get the effective porosity of the M.II in each column. The nonreactive tracer sodium bromide (NaBr, 30 mg/L in Milli-Q water) was injected into the column and the sampled outflow was analyzed by ion chromatography (ICS-1000, Dionex, AT) yielding the breakthrough curve of the tracer. From this curve, the V_P and the n_e were calculated, using the following equations:

$$V_P = \left(\left(\frac{t_1 - t_0}{(C/C_0)_1 - (C/C_0)_0}\right) * (0.5 - (C/C_0)_0) + t_0\right) * v_f - V_T \quad (3.2)$$

$$n_e = \frac{V_P}{V_C} \quad (3.1)$$

t_0 and t_1 are the two time steps (from the collected samples) before and after 50 % of the tracer breakthrough was measured, $(C/C_0)_0$ and $(C/C_0)_1$ are the incidental relative concentrations, v_f is the used flow rate (in the column experiments: mL/min), and V_C is the volume of the column. Because $C/C_0 = 0.5$ should occur (= 50 % of tracer breakthrough), when one V_P of the nonreactive tracer has eluted from the column (Stephens et al., 1998).

2. Before the GNP suspension could be injected, the columns were flushed with at least three V_P of F.I.m to equilibrate the system. Then the GNP injection was conducted, and the outflow was sampled, to test the suitable detection methods and to derive the GNPs mobility parameters.
3. When the plateau of the GNP suspension breakthrough was reached, the columns were flushed with F.I.m until all GNPs not clogged in or attached to the M.II were washed out. Again the outflow was sampled and analyzed with the suitable detection methods.
4. In the end the columns got dismantled: each two cm of the porous medium were taken out of the column separately, from bottom to top, to measure the total iron content. This was achieved by digesting the M.II portions with HCl (30 %) and HNO_3 (5 M), diluting it with Milli-Q water and filtering it through surfactant-free cellulose acetate filters (hydrophilic, 0.45 µm, 28 mm, Minisart® NML, Sartorius, DE) for total iron measurement via ICP-OES.

In total eight column experiments were conducted, always in duplicates, leading to a total of 16 columns (SI to SXVI). The experiments were performed with 1st GNP (1 g/L) and 2nd GNP suspensions (1 g/L and 10 g/L, see 3.1.1), and flow rates of 10.4 mL/min (corresponding to a flow velocity of 100 m/d), 5.8 mL/min (corresponding to a flow velocity 50 m/d of), and 1.06 mL/min (corresponding to a flow velocity of 10 m/d).

3.2.3 Particle transport & deposition

Transport and deposition of colloidal particles is controlled by advection-dispersion phenomena and by particle-collector and particle-particle interactions of physicochemical nature (Kretzschmar et al., 1999). Their transport and deposition in porous media is usually evaluated at minor particle concentrations (<30 mg/L) and modeled based on clean bed filtration theory (CFT) (Saleh et al., 2008; Tufenkji & Elimelech, 2004; Wang et al., 2008). However, very often deposition of colloidal suspensions, especially if higher particle concentrations are used (in the order of g/L), does not follow linear irreversible kinetics, considered in the CFT model, where detachment is supposed to be negligible. During transport of highly concentrated iron NP suspensions through porous media, deposition of a relevant fraction of the particles is an often observed effect. This deposition can be attributed to concurrent phenomena: (1) filtration and straining, where particles form aggregates in the pore space, getting filtered and/or strained by the porous media; (2) ripening, when particle-particle interactions cause deposited particles to attract suspended ones. These phenomena can become the prevailing mechanisms governing colloidal particle transport, affecting the hydrodynamic parameters of the porous medium, ultimately leading to clogging (Hosseini & Tosco, 2013; Jaisi et al., 2008; Phenrat et al., 2009).

The MNM1D code (Micro- and NP transport Model in porous media, in 1D geometry), an innovative colloid transport model, solves one dimensional transport with modified advection-dispersion-deposition equations to simulate transport of dispersed particles through saturated porous media (Hosseini & Tosco, 2013). The basis of the MNM1D code is the modified advection-dispersion equation, including a general exchange term for liquid solid phase transfer:

$$\begin{cases} n\dfrac{\partial c}{\partial t} + \rho_b \dfrac{\partial s}{\partial t} = nD\dfrac{\partial^2 c}{\partial x^2} - v\dfrac{\partial c}{\partial x} \\ \rho_b \dfrac{\partial s}{\partial t} = f(c) \end{cases} \tag{3.3}$$

c is the colloid number concentration in the liquid phase, s the number colloid concentration in the solid phase, ρ_b the bulk density of the solid matrix, D the hydrodynamic dispersion coefficient, v the darcyan velocity, and n the porosity of the packed bed. f(c) describes the mass transfer between solid and liquid phase and can

be written in different ways, matching the mechanisms, which have to be modeled. E.g. if a linear exchange term is hypothesized, f(c) becomes:

$$f(c) = nk_a - \rho_b k_d s \quad (3.4)$$

k_a is the attachment coefficient and k_d the detachment coefficient (Tosco & Sethi, 2009).

Modelling approach

The MNMs 2014 (Micro-and NP transport, filtration and clogging Model - Suite), a software tool that simulates colloid transport in porous media and merges the features of MNM1D and E-MNM1D (Enhanced Micro- and NP transport Model in saturated porous media, in 1D geometry, an extended version of MNM1D for simulation of transport of highly concentrated, non-Newtonian suspensions of colloidal particles), was used to model the GNPs column experiments. It allowed to estimate the colloidal transport kinetic coefficients (k_a and k_d) by fitting the modeled MNMs breakthrough curves to the GNP suspension breakthrough curves (using the total iron data) derived from the column experiments.

Mass balance

A mass balance of total iron (see 3.2.1.4) was established for each column. The amount of total iron injected (Fe^{tot}_{In}) into the columns was compared to the amount of total iron collected from the effluent samples (Fe^{tot}_{Out}), to estimate the amount of total iron, and thus the amount of GNPs retained in the columns after flushing with F.I.m. The recovery rate of the total iron ($rec_{Fe^{tot}}$) was calculated as follows:

$$Fe^{tot}{}_{In} = C_{In} * t_{in} * v_f \quad (3.5)$$

$$Fe^{tot}{}_{Out} = \sum_{i=1}^{n} C_i * t_i * v_f \quad (3.7)$$

$$rec_{Fe^{tot}} = \frac{Fe^{tot}{}_{Out}}{Fe^{tot}{}_{In}} \quad (3.6)$$

C_{In} is the total iron concentration of the injected GNP suspension, t_{In} the time of the injection, C_i and t_i are sample specific total iron concentration and sampling time, respectively for all samples (n) of each column experiment.

3.2.4 Detection of iron oxide NPs in the container experiment - pilot scale

As part of the NanoRem project, the overall goals of the pilot scale container experiment at VEGAS were:

1. to remediate a BTEX (toluene) plume utilizing GNPs,
2. to quantify the remediation (microbial degradation) efficiency and longevity of the GNPs, and
3. to evaluate transport and targeted deposition of GNPs in the subsurface.

The aim of this thesis, to test the elaborated GNPs detection methods in batch and lab scale experiments during the container experiment, appertained to number 3.

The container at VEGAS is 9.0 m long, 6.0 m wide, and 4.5 m high, and comprises 84 randomly distributed cuboids of medium (M.II) and coarse sand (for the characteristics of the sands see Table 3.5). The cuboids are arranged in three layers, seven rows, and four columns. The sampling ports are located on the orographic (regarding the groundwater flow) left side wall of the container. The sampling points that connect to the ports are homogeneously spread across the whole container. The 378 sampling points are serialized in six sampling planes (1-6), nine sampling rows (a-i), and seven sampling columns (A-G), as shown in Figure 3.6. The constant groundwater flow amounts to 1.5 m³/d (corresponding to a flow velocity / seepage velocity of 0.2 m/d) and the water table lies at ~3.7 m.

The GNP suspension (10 g/L) was injected through a well (diameter of 10 cm) located within layer 1 and 2 (see Figure 3.6). Prior to the injection a contaminant plume

of toluene (20 mg/L) was established inside the container, and a tracer test with uranine (fluorescein, 30 g/L, 1.33 m³) was carried out, to validate the permeability distribution of the container.

To detect the GNPs after injection and to map their movement within the container a sampling plan had to be designed, as sampling at all 378 sampling ports would not have been possible. A hydraulic model of the container at VEGAS was built, to get an idea of the groundwater flow and to decide the location of the sampling points.

Table 3.5: Characteristics of the sand types used in the container experiment (CE).

Characteristics of the sand types		
	Medium sand	**Coarse sand**
Grain size distribution	0-4 mm	0.2-8 mm
Porosity	n = 0.35	n = 0.4
Particle density	2.65 x 10^3 kg/m³	2.65 x 10^3 kg/m³
Bulk density	1.72 x 10^3 kg/m³	1.59 x 10^3 kg/m³
Permeability	k = 4.1 to 14.3 x 10^{-5} m²	k = 35.7 to 61.2 x 10^{-5} m²
Hydraulic conductivity	K = 4 x 10^{-4} m/s (constant head permeameter) K = 14 x 10^{-4} m/s (tracer in CE)	K = 35 x 10^{-4} m/s (constant head permeameter) K = 60 x 10^{-4} m/s (tracer in CE)

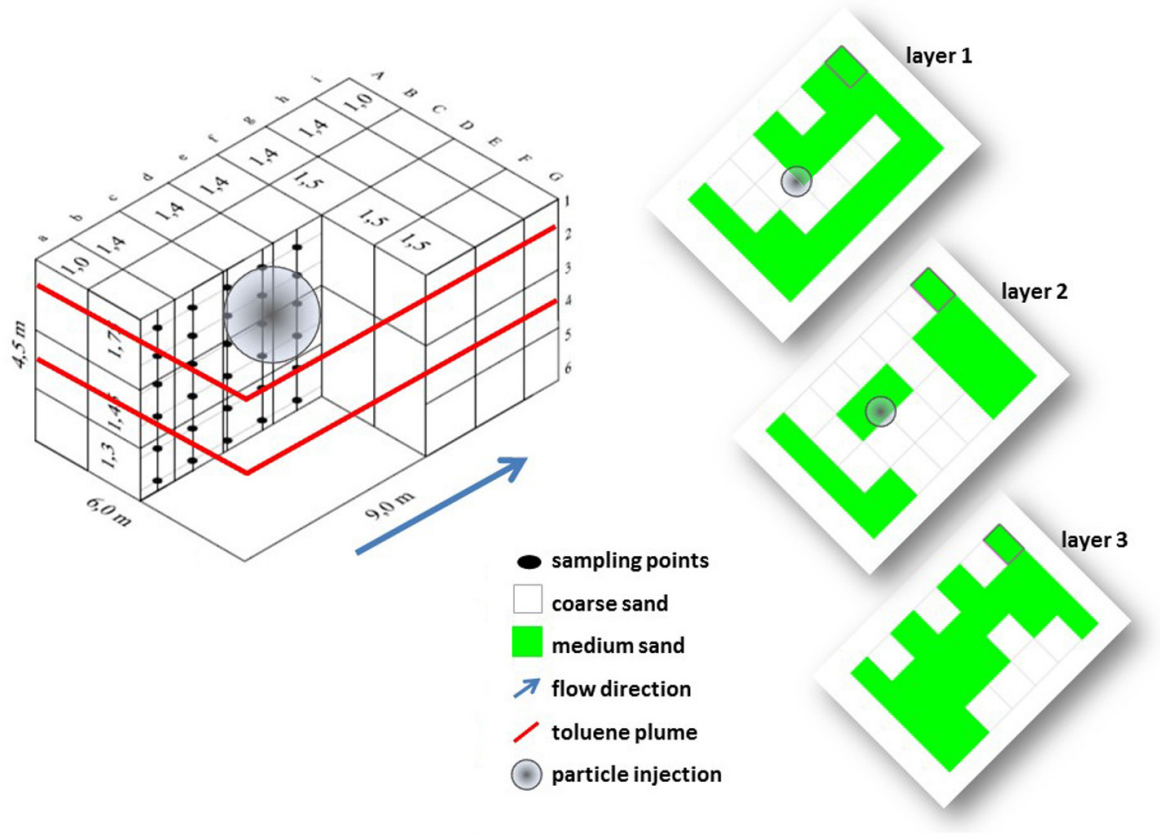

Figure 3.6: Sketch of the VEGAS container, with the position of the toluene plume (between the red lines), the GNP injection (well), the sampling points within the container, and the distribution of the cuboids of the two different sand types in the three layers (sketch partially provided by VEGAS).

A hydraulic model of the VEGAS container was built with Processing Modflow™ (PM80400, Simcore Software) creating a virtual clone of the real container (see above). In a first step just the groundwater flow was modeled. With the advection model PMPATH (within Processing Modflow™) particles (hypothetical particles without mass, acting like a conservative tracer) were tracked, to visualize flow paths. In a second step, the injection well was added, pumping with a flow rate of 0.033 m³/h (corresponding to a flow velocity of 100 m/d). In this step, the particle tracking was used to reveal the changes in flow paths within the container due to the injection.

4 Results and discussion

4.1 Suitable techniques for iron oxide NP characterization and detection

The testing of available detection methods lead to a list of suitable and non-suitable techniques (see Table 4.1):

- **Laser diffraction** (Mastersizer) worked fine for the particle characterization and detection in batch scale experiments, but for detection of GNPs in column experiments, the amount of the single sample (5.25 ±0.06 mL) was too small for that method. In addition, after the measurement the sample is lost. The instrument is too bulky to bring to a field site, so this method was out of question for the container experiment.
- **Dynamic light scattering** (Zetasizer) proved to be suitable for the characterization and detection of the GNPs on all three experimental scales. Only the measured hydrodynamic diameters (Z-Average) of GNPs in suspensions with particle concentrations lower than 0.01 g/L were not in the range of confidence (e.g. to high polydispersity index (PDI) or to low count rate).
- **Laser obscuration time** (EyeTech) was not the right measurement principle for the GNPs, since the size of the particles (316 nm for 1st GNP and, 215 nm for 2nd GNP, see 3.1.1) is below the detection limit of the EyeTech (>600 nm).
- **Electrophoretic light scattering** (Zetasizer) worked fine to characterize the GNPs and to detect them in batch scale experiments.
- **The 90° scatter method** (Turbidity meter) proved to be a fine principle to detect the GNPs and to determine their particle concentration in the batch, lab, and pilot scale experiments in suspensions with concentrations between 0.01 and 1 g/L. It also worked quite well for suspensions with higher

concentrations, if they were diluted with Milli-Q water (1:10) for the measurement.

- **Inductively coupled plasma optical emission spectrometry** (ICP-OES) measuring the total iron of the samples to detect the GNPs, worked for particle detection on all three scales. The iron in the samples had to be digested before measurement. Since the ICP-OES is integrated into the laboratory it is not applicable in the field. However, if the samples are stable, it is a good choice because of its automated measuring.
- **Ultraviolet-visible spectrophotometry** (UV-Vis) was not suitable for GNP detection or characterization, because of too much interference with other compounds, e.g. humic acids in the samples.

Table 4.1: Suitability of the instruments tested to characterize and detect the GNPs (+ suitable, - not suitable).

Property	Instrument	Suitability	Outcome
Size	Mastersizer	+	Too much sample needed, too bulky
	Zetasizer	+	Working
	EyeTech	-	GNPs size below detection limit
Surface charge	Zetasizer	+	Working
Concentration	Turbidity meter	+	Working for concentrations 0.01 - 1 g/L
	ICP-OES	+	Pretreatment before measuring in the lab
	UV-Vis	-	Too much interference

4.1.1 First batch goethite nanoparticles

The determination of the particle concentration of the 1st GNP stock solution showed that it contained 3.56 ±0.09 % GNPs, posing a ratio of 2.81 between a 10 g/L solution and the actual stock solution. This means that for 100 mL of a 1 g/L GNP suspension 2.81 g of the stock solution had to be added to 97.19 g of Milli-Q water or F.I.m.

The results of the characterization of the 1st GNPs in a 1 g/L dilution in Milli-Q water and in a 1 g/L dilution in F.I.m are depicted in Table 4.2.

4.1.2 Second batch goethite nanoparticles

The determination of the particle concentration of the 2nd GNP stock solution showed that it contained 9.23 ±0.02 % GNPs, presenting a ratio of 1.08 between a 10 g/L solution and the actual stock solution. This means that for 100 mL of a 1 g/L GNP suspension 1.08 g of the stock solution had to be added to 98.92 g of Milli-Q water or F.I.m.

The results of the characterization of the 2nd GNPs in a 1 g/L dilution in Milli-Q water and in a 1 g/L dilution in F.I.m can be seen in Table 4.2.

Table 4.2: Parameters of the 1st and 2nd GNPs in a dilution of 1 g/L in Milli-Q water and F.I.m. and their standard deviation.

	1st GNPs 1 g/L, Milli-Q	1st GNPs 1 g/L, F.I.m	2nd GNPs 1 g/L, Milli-Q	2nd GNPs 1 g/L, F.I.m
Z-Average [nm]	238.7 ±2.4	246.7 ±2.7	200.1 ±2.2	228.0 ±4.4
Zeta pot. [mV]	-50.2 ±0.8	-32.5 ±1.3	-48.8 ±0,6	-22.8 ±1.4
Total iron [mg/L]	303.2 ±11.3	191.3 ±19.8	50.0 ±9.0	63.67 ±10.1
Turbidity [NTU]	1049 ±37	1589 ±44	885 ±35	940 ±65
EC [µS/cm]	222 ±2	458 ±2	84 ±3	347 ±5
pH	9.0	8.2	9.3	8.0
TOC [mg/L]	232.8 ±11.4	232.8 ±11.4	73.4 ±6.5	73.4 ±6.5

4.1.3 Effect of ionic strength on iron oxide NPs size

The changes of parameters between the GNPs in the two different waters (see Table 4.2) can be attributed to the effect of the ionic strength on the GNPs. This can be described by the Derjaguin-Landau-Verwey-Overbeek (DLVO) theory, applied to calculate and model interacting forces like electrostatic double layer and Van der Waals forces between charged surfaces, interacting through a liquid medium (Elimelech et al., 1995). The DLVO theory shows in fact that the zeta potential of particles drops with an increase in ionic strength. With rising ionic strength in the liquid medium, the diffuse layer surrounding the particle gets compressed (double layer

compression) and the stern layer potential gets decreased, resulting in a drop of the actual zeta potential towards a more positive value (Gregory, 2004).

The increase in particle size can also be attributed to the double layer compression, by leading to a shorter range of the repulsive forces (charge screening), and thereby increasing the likelihood of a close approach of particles due to Van der Waals forces, leading to aggregation (Gregory, 2004). A minor increase in particle size with higher ionic strength was observed for both 1st GNPs and 2nd GNPs, but not with such an impact as expected. Apparently, the presence of HSs in the suspension provides a means of controlling the state of aggregation of the GNPs, against the effect of ionic strength, by forming a charged external interaction with the particle surface (Grillo et al., 2015; Johnson et al., 2009; Maurer-Jones et al., 2013).

4.2 Detection of iron oxide NPs in batch scale

4.2.1 Turbidity vs total iron - batch scale

The turbidity of the different concentrations (see 3.1.1) of 1st and 2nd GNP suspensions in Milli-Q water and F.I.m was compared to their total iron content. The calibration of turbidity and total iron for the different particle concentrations delivered good results:

- turbidity of 1st GNP suspension (in F.I.m) corresponds to the particle concentration with a coefficient of determination of $R^2 = 1.00$
- turbidity of 2nd GNP suspension (in F.I.m) corresponds to the particle concentration with $R^2 = 1.00$,
- total iron of 1st GNP suspension (in F.I.m) corresponds to the particle concentration with $R^2 = 1.00$,
- only total iron of 2nd GNP suspension (in F.I.m) shows a rather poor agreement with the particle concentration with solely $R^2 = 0.76$ (see 3.2.1.3 and Figure 3.3, and 3.2.1.4 and Figure 3.4).

Therefore it was assumed that the turbidity would coincide with the total iron similarly good. This was the case for the 1st GNP suspensions in both Milli-Q water and F.I.m ($R^2 = 0.99$ and $R^2 = 1.00$. However, the coincidence for the 2nd GNP suspensions in

Milli-Q water and F.I.m, was less accurate (R^2 = 0.92 and R^2 = 0.93), as can be seen in Figure 4.1. Whereas turbidity and total iron corresponded well for low concentrations between 0.01 and 0.1 g/L (R^2 = 1.00 and R^2 = 0.99), only higher concentrations deviate rather strongly.

Since this was observed in both Milli-Q water and F.I.m dilutions it cannot be attributed to effects from the ionic strength, but most probably to the issues in digesting all of the iron in 2nd GNP suspensions with concentrations higher than 0.1 g/L. The attempt to use greater amounts of HCl and HNO_3 than previously used to digest all the iron in the 2nd GNP suspensions was fruitless and just let to the same results. Further, after adding the acids (impartial to the amount) a precipitate formed.

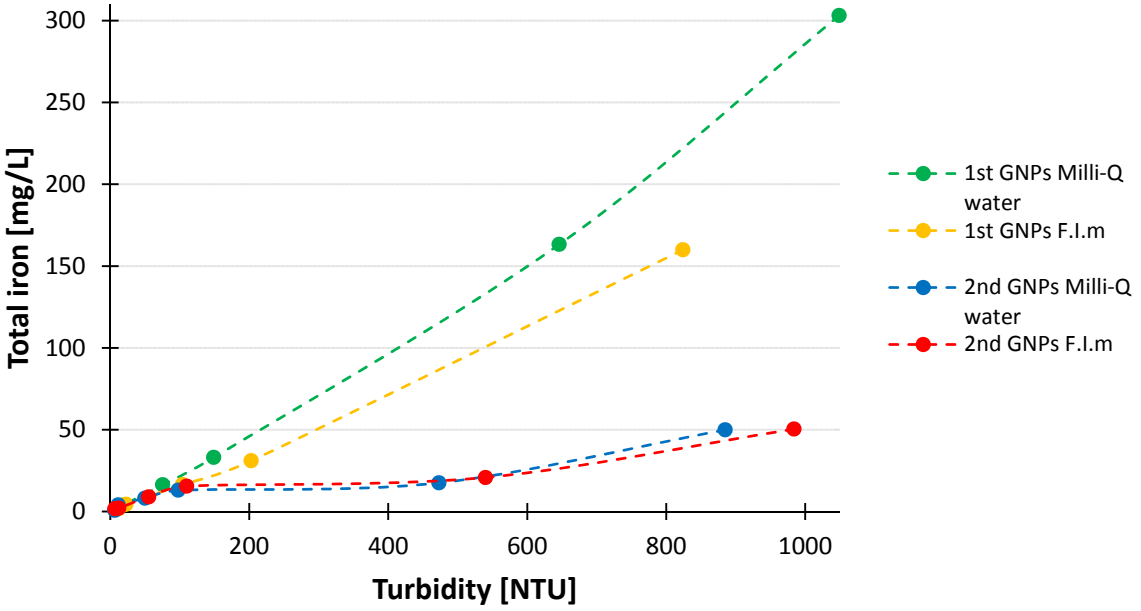

Figure 4.1: Turbidity against total iron of 1st and 2nd GNP suspensions in Milli-Q water and F.I.m. The dashed lines are plotted to guide the readers' eyes, without suggesting exact trends.

4.2.2 Effect of pH on iron oxide NPs sedimentation

The sedimentation of 2nd GNP suspensions during acid digestion could be associated with a pH drop correlated to the addition of the acids. The 2nd GNP suspensions in F.I.m exhibited a pH of 8.06 ±0.07 and it dropped most likely (pH after addition of the acids was not measured) to ~7.8 (or lower), the point of zero charge

(PZC). Below the PZC iron oxide NPs are positively charged and above it, they are negatively charged, whereas around the PZC the particles are not, or the least charged. According to the DLVO theory that leads to no, or very little repulsion forces between the particles, increasing the formation of aggregates and promoting sedimentation (Baalousha, 2009). Additionally, the HSs, preventing the GNPs from aggregating, tend to be less soluble with decreasing pH. By adding the acids to the samples, a chain reaction was triggered: the pH of the suspension decreased, removing some of the HSs from it and increasing the formation of NP aggregates. The decline in available HSs further led to a decrease of the stability of the NPs forming even more and even bigger aggregates.

This chain reaction removed GNPs, and thereby iron from the suspension and led to the fact that not all of the total iron could be measured. The reason why the same effect was not showing on the 1st GNP suspensions is probably due to the triple amount of HSs (see Table 4.2, TOC), able to compensate for the effect of the PZC and to make up for the loss of HSs (due to the pH drop).

4.2.3 Particle size - batch scale

The size of the 1st and 2nd GNPs in the different dilutions with Milli-Q water and F.I.m (see 3.1.1) was determined via DLS and compared to each other, showing that:

- The size of 1st GNPs both in Milli-Q water and F.I.m did not deviate much from each other over the different concentrations, whereas the size of the 2nd GNPs in the different concentrations in Milli-Q water was quite diverse from the ones in the different concentrations in F.I.m (the gap between them getting smaller with higher concentrations).
- All, 1st and 2nd GNP dilutions, no matter if in Milli-Q water or F.I.m, showed a rather noticeable increase in size for the 1.5 g/L concentration. Solely for the 1st GNPs in F.I.m that increase was not that prominent, admittedly discernible, but still within the standard deviation (SD) concerning the other concentrations.
- The size of the 1st and 2nd GNPs, in the 2 g/L concentrations were almost the same, no matter the dilution water (see Figure 4.2).

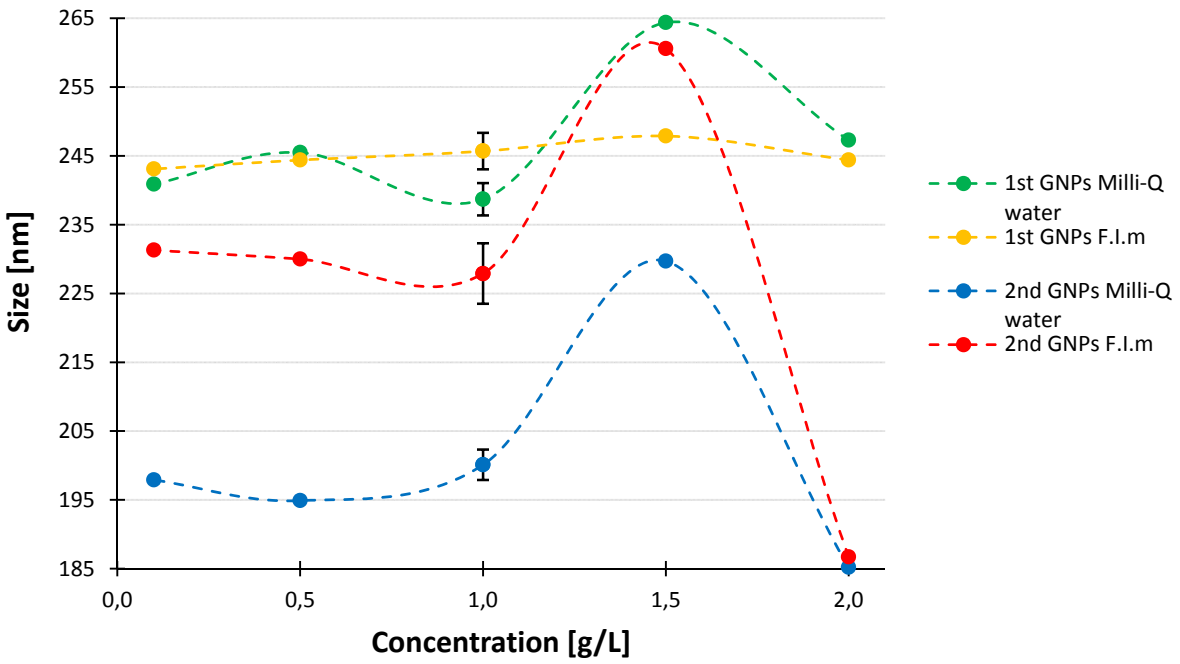

Figure 4.2: Size of 1st and 2nd GNPs in Milli-Q water and F.I.m over the different particle concentrations from 0.1 to 2.0 g/L. The error bars represent the SD of the GNPs in the 1 g/L concentrations. The dashed lines are merely for clarity, and don't suggest exact trends.

4.2.4 Effect of particle concentration on iron oxide NPs size

It is known that an increase in particle concentration increases the aggregation and therefore the measured size of the particles, due to the higher probability of particle collision (Baalousha, 2009; Maximova & Dahl, 2006).

This explains the increase in particle size of ~30 nm between the 1 and 1.5 g/L suspensions. For suspensions below 1 g/L the particle concentration is probably too low, for this effect to be noticeable. The drop in particle size between the 1.5 and 2 g/L suspensions cannot be explained with this concentration effect alone. Between 1.5 and 2 g/L there is an increase in particle size, due to the concentration effect, leading to fast sedimentation of "big" aggregates, and to actual particle concentrations of the suspensions of 0.1 g/L or lower. This results in the measurement of small particle sizes again.

Sedimentation rates

The sedimentation rate, determined via MLS for 1 and 10 g/L concentrations (only in F.I.m), was 0.32 ±0.05 mm/hr or indeterminable. The difficulties in determining the sedimentation rates were due to the HSs in the suspensions, responsible for the dark color; if the HSs were not bound to the GNPs they did not settle, making it difficult to measure the sedimentation rate of the particles.

4.2.5 Zeta potential - batch scale

The zeta potential of the 1st and 2nd GNPs in the different dilutions with Milli-Q water and F.I.m (see Figure 4.3) was determined via ELS and compared to each other, showing that:

- Zeta potential of 1st and 2nd GNPs in Milli-Q water became slightly less negative with increasing particle concentration (1st GNPs about 14 mV and 2nd GNPs about 2 mV), but was generally more negative than in F.I.m.
- Zeta potential of the 1st and 2nd GNPs in F.I.m became more negative with increasing particle concentration (1st GNPs about 12 mV and 2nd GNPs about 8 mV), but being generally less negative than in Milli-Q water.

4.2.6 Effect of particle concentration on iron oxide NPs zeta potential

That the GNPs exhibit a less negative zeta potential in the F.I.m compared to the GNPs in Milli-Q water was expected, since the ions in the F.I.m screen the surface charge of the GNPs (Laumann et al., 2013). The ionic strength (see 4.1.3) was weaker with increasing particle concentration (the same amount of ions have to screen more surface charges), explaining the increase in negative zeta potential with higher particle concentrations. The decrease in negative zeta potential for the GNPs in Milli-Q water, with increasing particle concentration, must not be an actual decrease at all as: (1) it does not follow a linear decrease (1st GNPs only $R^2 = 0.80$ and 2nd GNPs even less

R^2 = 0.41) and (2) the standard deviation of ±8.3 mV for these zeta potential measurements is bigger (for 2nd GNPs) or almost as big (for 1st GNPs) as the decrease in negative zeta potential.

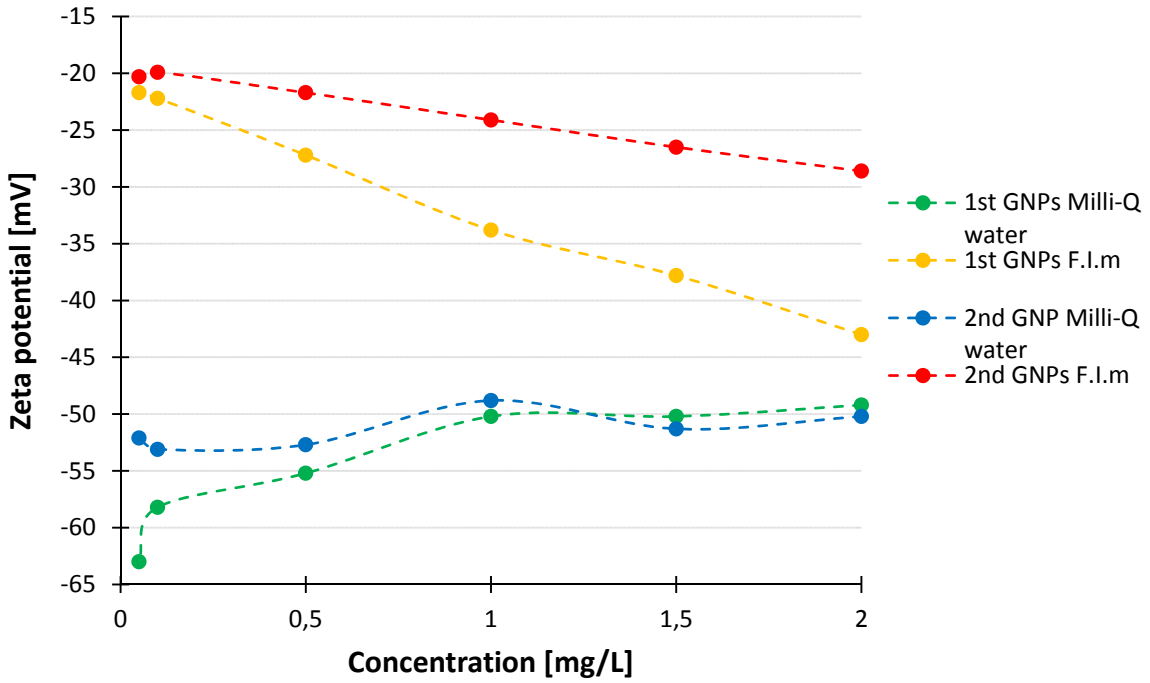

Figure 4.3: Zeta potential of 1st and 2nd GNPs in Milli-Q water and F.I.m over the different particle concentrations from 0.1 to 2.0 g/L. The dashed lines are plotted to guide the readers' eyes, without suggesting exact trends.

4.3 Detection of iron oxide NPs in column experiments - lab scale

The tracer experiments conducted in a first step of each column experiment resulted in a pore volume of V_P = 33.48 ±0.97 mL for each column, and an effective porosity of n_e = 31.00 ±0.90 % for the M.II in that columns. The slight difference between the single columns of 0.97 mL or 0.90 % can be accredited to the difficulty of packing each column exactly the same with the heterogeneous M.II.

Not all conducted column experiments will be presented here. For a better comprehension only representative experiments for the different batches of GNPs, particle concentrations, and flow rates will be discussed:

- **SVII** and **SVIII**: 1st GNP suspension with a particle concentration of 1 g/L was injected with a flow rate of 1.06 mL/min (flow velocity of 10 m/d).
- **SIX** and **SX**: 2nd GNP suspension with a particle concentration of 1 g/L was injected with a flow rate of 10.5 mL/min (flow velocity of 100 m/d).
- **SXIII** and **SXIV**: 2nd GNP suspension with a particle concentration of 10 g/L was injected with a flow rate of 10.5 mL/min (flow velocity of 100 m/d).
- **SXV** and **SXVI**: 2nd GNP suspension with a particle concentration of 10 g/L was injected with a flow rate of 1.06 mL/min (flow velocity of 10 m/d).

The breakthrough curves for the GNP suspensions, represented by total iron and turbidity data of the column effluents, in the chosen column experiments are shown in Figure 4.4. Effluent concentration (C) in relation to influent concentration (C_0) were plotted as a function of pore volume, whereas turbidity data were depicted as continuous and total iron data as dashed lines.

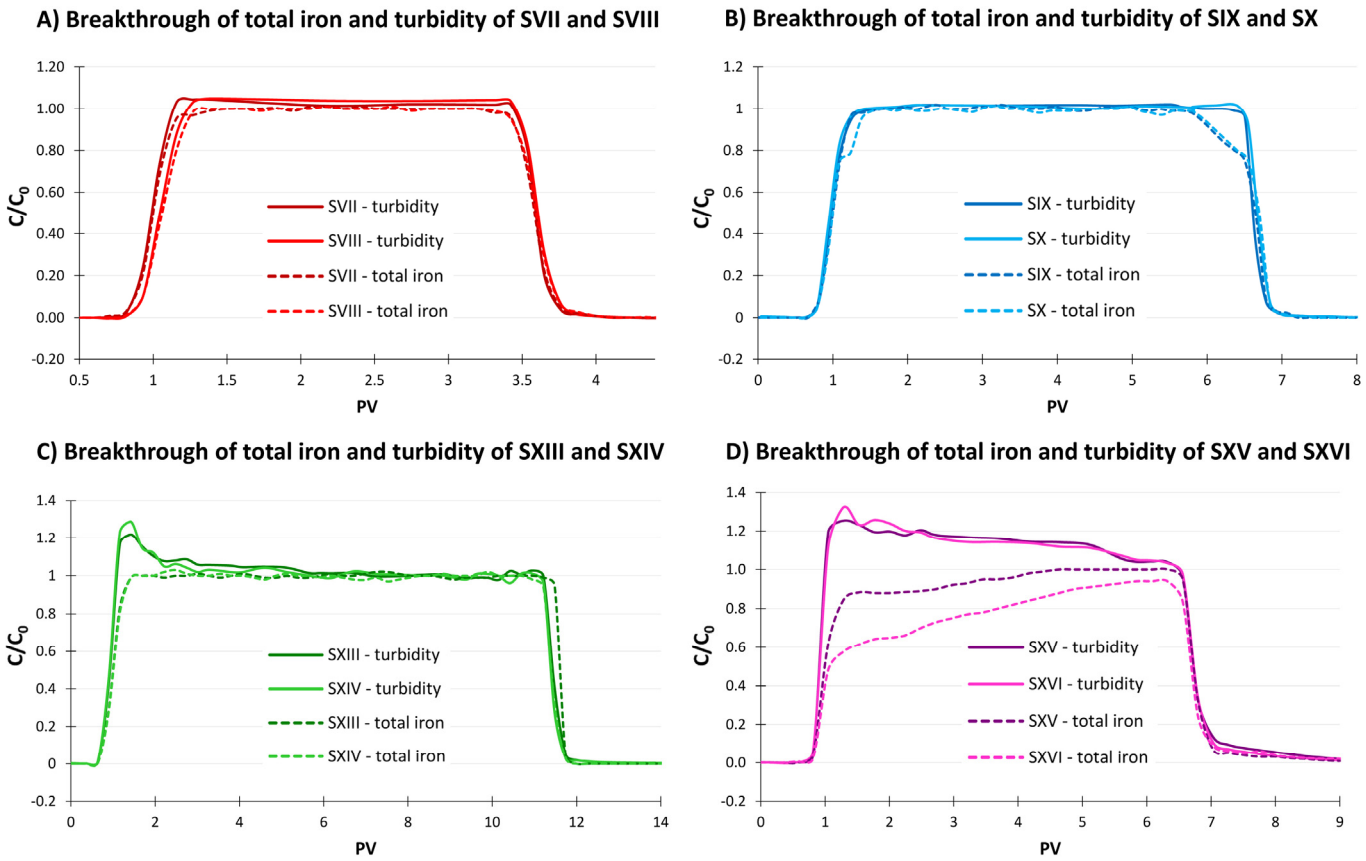

Figure 4.4: Breakthrough curves of GNP suspensions, represented by total iron and turbidity data of the column effluents as a function of pore volume of the columns. (A) SVII and SVIII (1st GNPs, 1 g/L, 1.06 mL/min), (B) SIX and SX (2nd GNPs, 1 g/L, 10.5 mL/min), (C) SXIII and SXIV (2nd GNPs, 10 g/L, 10.5 mL/min), and (D) SXV and SXVI (2nd GNPs, 10 g/L, 1.06 mL/min).

4.3.1 Total iron - lab scale

As can be seen in Figure 4.4, total iron is a solid tool to track the GNPs, and delivers nice breakthrough curves. Discrepancies between the duplicates (two columns were used simultaneously during each experiment) are probably due to the variations in packing the columns. These discrepancies supposedly led to the development of different flow paths through the porous medium (preferential flow), resulting in the observed distinctions. The most pronounced difference between two duplicates (SXV and SXVI) can be seen in D (see Figure 4.4), where the effect of the inconsistent column packing and preferential flow gets apparently enhanced by the slow flow rate (1.06 mL/min) and the high particle concentration (10 g/L). The buildup of preferential flow in SXV and SXVI could even be seen during the experiment (see Figure 4.5). The unusual drop of total iron during the flushing of the columns SIX and SX in B (see

Figure 4.4) was not observed in any of the other experiments, but since it is identical for both columns, heterogeneous packing and an error in sampling during the experiment or the measurement can be excluded. This gets further substantiated by the turbidity data, where this unusual drop was not measured, and leaves it as an open question.

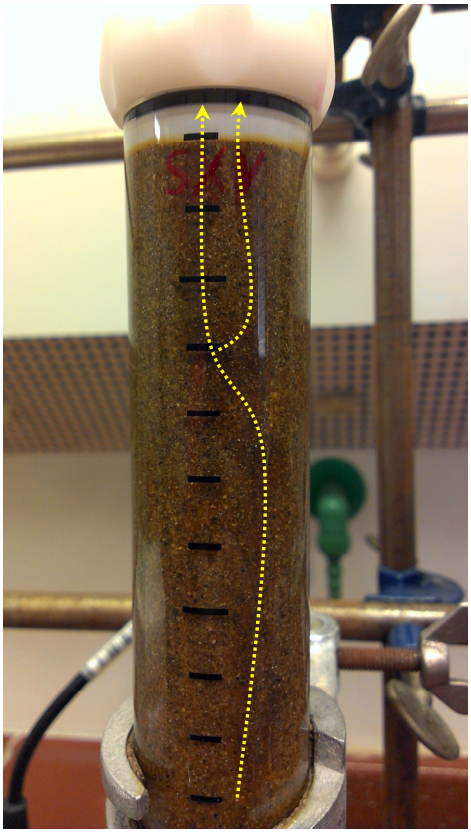

Figure 4.5: On this photo of column SXV, taken during the experiment, a preferential flow path can be seen (marked in yellow, the arrows are indicating the flow direction). Due to the higher particle concentration of the suspension following the flow paths, they appear darker then the surrounding material.

When comparing the different experiments to each other (A, B, C, and D in Figure 4.4) the shapes of the breakthrough curves of total iron do not show differences in the different batches of GNPs, flow rate, or particle concentration (A,B, and C). Except for D, where low flow rate (1.06 mL/min) and high particle concentration (10 g/L) are combined. In all experiments the plateau of the breakthrough curve ($C/C_0 = 1$) was reached, right after one PV of the columns (filled with F.I.m) has been exchanged with GNP solution, but not in D. In D, right after 1 PV was exchanged, the value of C/C_0 only reached 0.5 (SXVI) and 0.7 (SXV), respectively. From there, the C/C_0 rose very slowly, until the plateau was attained: for SXVI at $C/C_0 = 1$, after 4.5 PVs where

exchanged and for SXV at C/C_0 = 0.94 after 5.8 PVs where exchanged. This at first fast (like in the other experiments), but then quite slow ascent can be affiliated to filtering/straining or ripening effects (see 3.2.3) of the particles within the porous medium.

4.3.2 Turbidity - lab scale

Like total iron, turbidity seems to work well in detecting the GNPs. The turbidity breakthrough curves are very similar to the ones of total iron (see Figure 4.4): almost identical for the experiments with the low concentration suspensions (1 g/L, A: SVII and SVIII, and B: SIX and SX) and the high flow rate (10.5 mL/min, B: SIX and SX, and C: SXIII and SXIV). Only the experiment with the high concentration suspension and the low flow rate (10 g/L, 1.06 mL/min, D: SXV and SXVI) differs significantly, in comparison to both the total iron (in D) and the other turbidity curves (in A, B, and C). The peaks in turbidity, swiftly after 1 PV of suspension was injected into the columns, are quite distinct (in C) if not to say predominant (in D) in the high concentration experiments, whereas in the low concentration experiments they are almost not existent (in A and B). Apparently, despite the attempt to get rid of any background turbidity by flushing the columns thoroughly before the experiments, there was some of it left in the columns. Presumably a fine portion of the M.II which was not to be flushed out with water, got washed out by GNP suspensions. If this was due to the higher density of the suspensions in comparison to water or if the HSs in the suspension mobilized fines (comparable to NP stabilization by HSs see 1.2.1) was not evaluated. However, this explains why the peaks are so pronounced in the experiments with the high concentration suspension, whose density and HS concentration are higher than from the low concentration suspensions. The difference in the turbidity peaks associated with the flow rate (between C and D) is merely the way the peak flattens to the plateau. It takes more or less 6 PV in both experiments, but where in C the decline seems to be logarithmic, in D it appears to be linear.

4.3.3 Turbidity vs total iron - lab scale

When comparing turbidity data with total iron data of the samples of the single column experiments, ideally the data points should string on a straight line, as they do in graph A in Figure 4.6 (SVII and SVIII, $R^2 = 0.99$). However, for B (SIX and SX, $R^2 = 0.97$), C (SXIII and SXIV, $R^2 = 0.91$), and D ((SXV and SXVI, $R^2 = 0.86$) this is true only for lower values. For higher turbidity and total iron values, the plotted points scatter rather widely. As already mentioned in 4.2.1 this phenomenon has to do with the problematic of fully digesting all of the iron in the 2nd GNP suspensions. Since this was not an issue with the 1st GNP suspension, in A the scattering does not show. In B, where only a low concentration (1 g/L) suspension was used the scattering is confined to the upper end. In C and D, where high concentration (10 g/L) suspensions were injected, the issue presents itself already earlier due to the error in iron digestion, but also due to the turbidity peaks in the beginning of the injections, adding some background turbidity to the true GNPs values (see 4.3.2 and Figure 4.4).

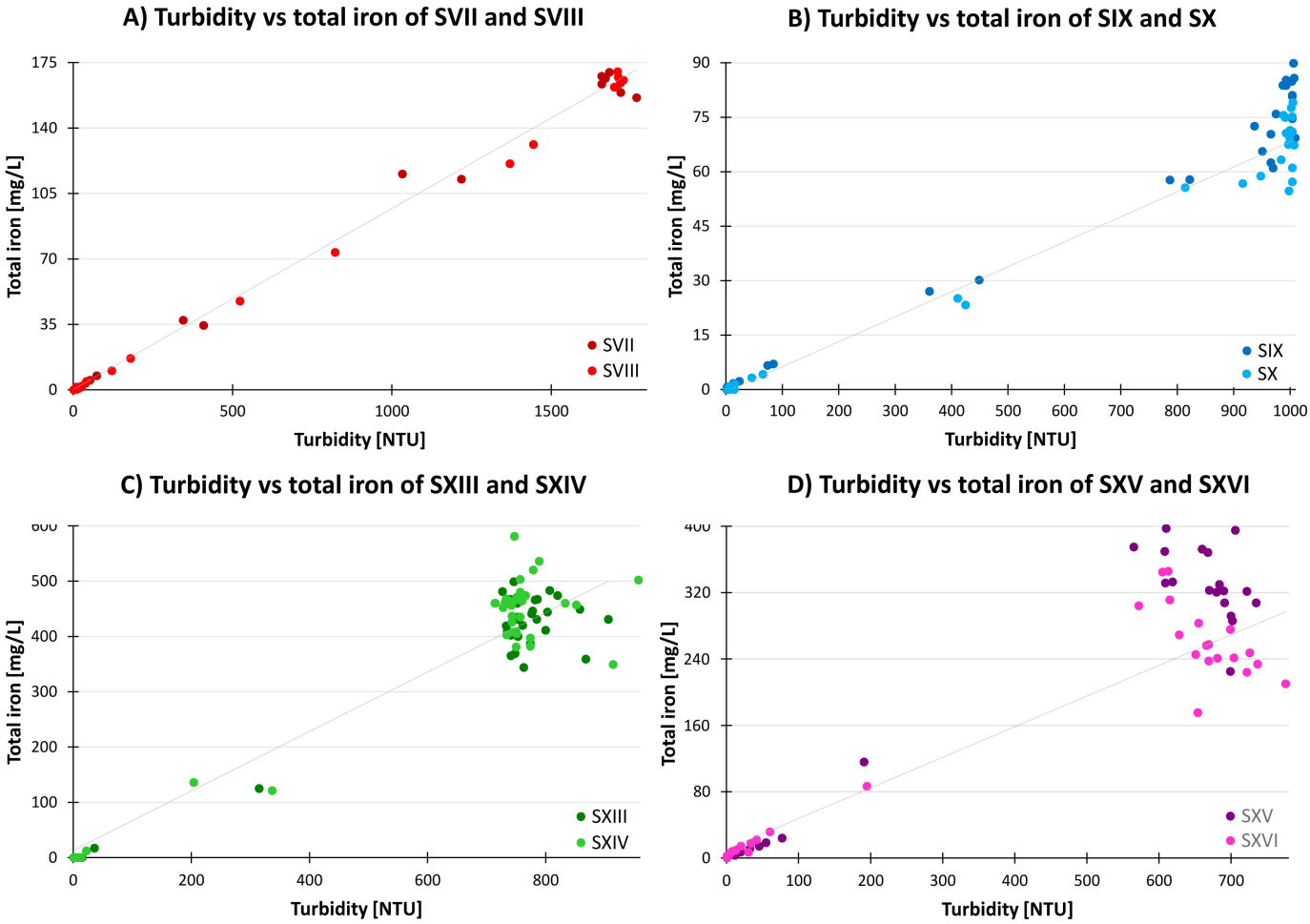

Figure 4.6: Turbidity against total iron data of the samples from the columns. (A) SVII and SVIII (1st GNPs, 1 g/L, 1.06 mL/min), (B) SIX and SX (2nd GNPs, 1 g/L, 10.5 mL/min), (C) SXIII and SXIV (2nd GNPs, 10 g/L, 10.5 mL/min), and (D) SXV and SXVI (2nd GNPs, 10 g/L, 1.06 mL/min).Trend lines in light gray.

4.3.4 Particle size - lab scale

Looking at the particle size, or rather the change of the particle size during the column experiments, reveals a certain pattern, mutual to all experiments (see Figure 4.7). The small difference between the duplicates themselves can be connected to the difficulty of packing both columns exactly the same, leading to different flow paths and regimes inside the columns. The only major difference between the experiments is the particle size itself, depending on the different GNP batches or particle concentration. The first particles eluding the column are quite large (~450 nm in A, ~500 nm in B, and ~400 nm in C and D), but that size diminishes rather fast and reaches more or less a plateau (~250 nm in A, ~350 nm in B, and ~150 nm in C and D) after 1.5 to 2 PV were

exchanged. When the columns get flushed with F.I.m the size of the particles coming out of the columns changes again. After the flushing starts, there is a short peak in the particle size. After that peak (corresponding to the end of the plateau in the breakthrough curves of total iron and turbidity), the particle concentration in the samples is, in most cases, too low to have any validity. All this changes in size can easily be explained with the effect of concentration (see 4.2.4). The case that the particles in C and D are smaller than in B, what they should not be, considering the effect of concentration, is entirely owed to the fact that the samples from C and D (SXIII, SXIV, SXV, and SXVI) had to be diluted (1:10 with Milli-Q water) to be measured (see 3.2.1.1).

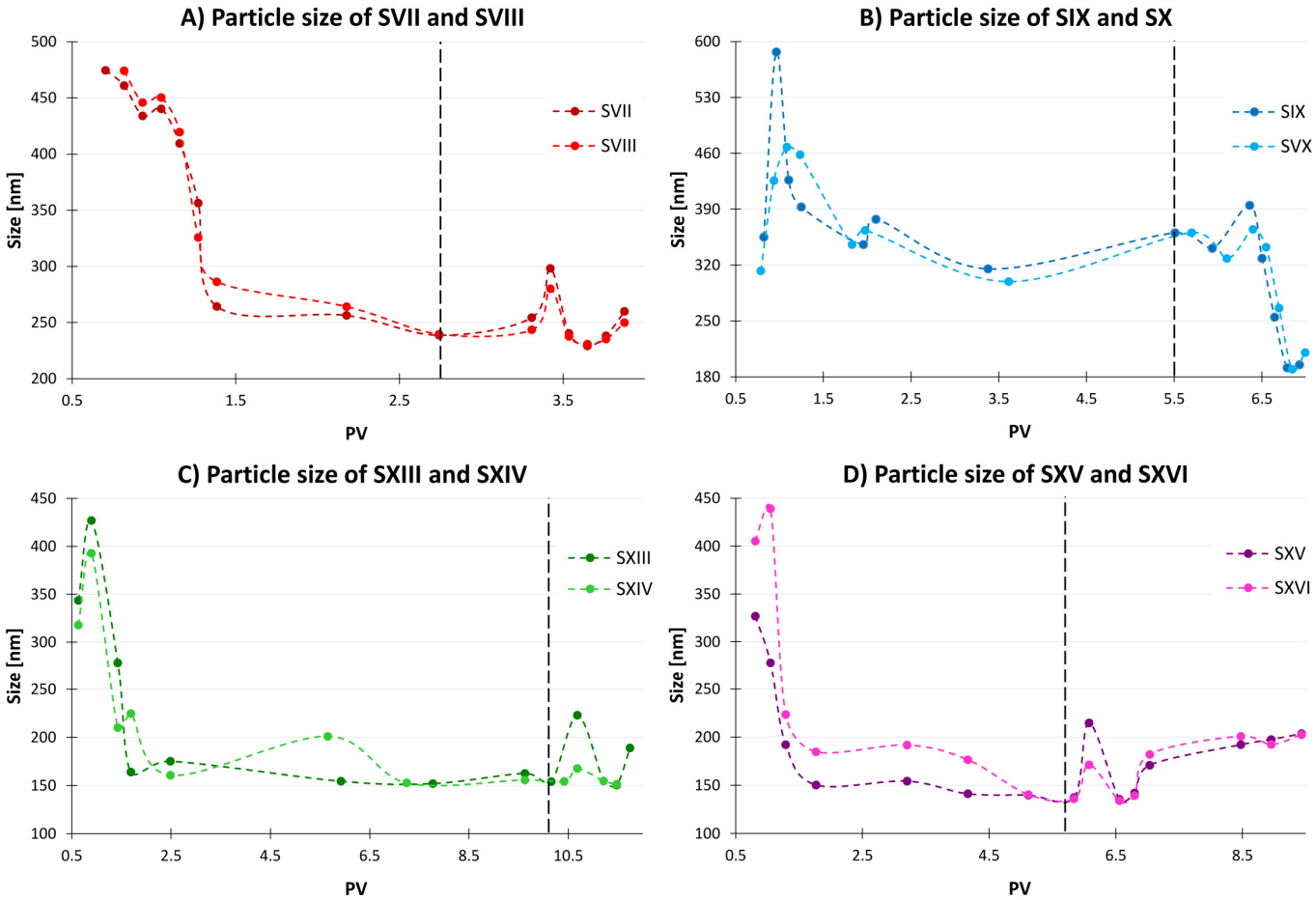

Figure 4.7: The size of the GNPs as a function of the PV exchanged within (A) SVII and SVIII (1st GNPs, 1 g/L, 1.06 mL/min), (B) SIX and SX (2nd GNPs, 1 g/L, 10.5 mL/min), (C) SXIII and SXIV (2nd GNPs, 10 g/L, 10.5 mL/min), and (D) SXV and SXVI (2nd GNPs, 10 g/L, 1.06 mL/min).The dashed black lines mark the change from GNP suspension injection to flushing with F.I.m. The colored dashed lines are merely for clarity, and don't suggest exact trends.

4.3.5 Pressure

The pressure measured during the column experiments as an indicator for clogging phenomena recorded no increase in pressure drop. This means that there was no clogging going on, at least not to an amount the pressure probes would have been able to detect.

4.3.6 Mass balance

The mass balance of the column experiments showed that more or less the same amount of GNPs injected into the columns was later flushed out again (see Table 4.3). Some discrepancies where observed between the duplicates. This time the reason was to be found in the difficulty to digest all the iron of the GNPs and to get exact total iron values. Only in column SXVI (with a recovery rate of 72 ±5 %) and SXV (with a recovery rate of 92 ±5 %) 28 ±5 % and 8 ±5 % of the particles got retained (filtered/strained or ripened) respectively. This can also be seen in their total iron breakthrough curves in Figure 4.4 D. For all the other columns the recovery rate is assumed to be more or less 100 % (allowing an error range of 5 %), this is also suggested by the total iron breakthrough curves.

Table 4.3: The recovery rates from the mass balance (total iron) of the GNPs injected into the columns SVII, SVIII, SIX, SX, SXIII, SXIV, SXV, and SXVI.

	Recovery rate [rec^{Fe}_{tot}]	
SVII - SVIII	0.94 ±0.05	0.91 ±0.05
SIX - SX	1.05 ±0.05	0.92 ±0.05
SXIII - SXIV	1.00 ±0.05	1.04 ±0.05
SXV - SXVI	0.92 ±0.05	0.72 ±0.05

4.4 Particle transport

4.4.1 Transport models

The same four column experiments (in total 8 columns) as in 3.2.2 will be presented here, to have the complete set of the same eight columns. There was a great agreement between models and actual breakthrough curves of the total iron in the column experiments after fitting the model by varying the attachment and the detachment coefficients (k_a and k_d), to the experimental data (see Figure 4.8):

- **SVII** and **SVIII** by R^2 = 1.00 and R^2 = 1.00,
- **SIX** and **SX** by R^2 = 0.99 and R^2 = 0.99,
- **SXIII** and **SXIV** by R^2 = 0.99 and R^2 = 1.00,
- **SXV** and **SXVI** by R^2 = 0.98 and R^2 = 0.97.

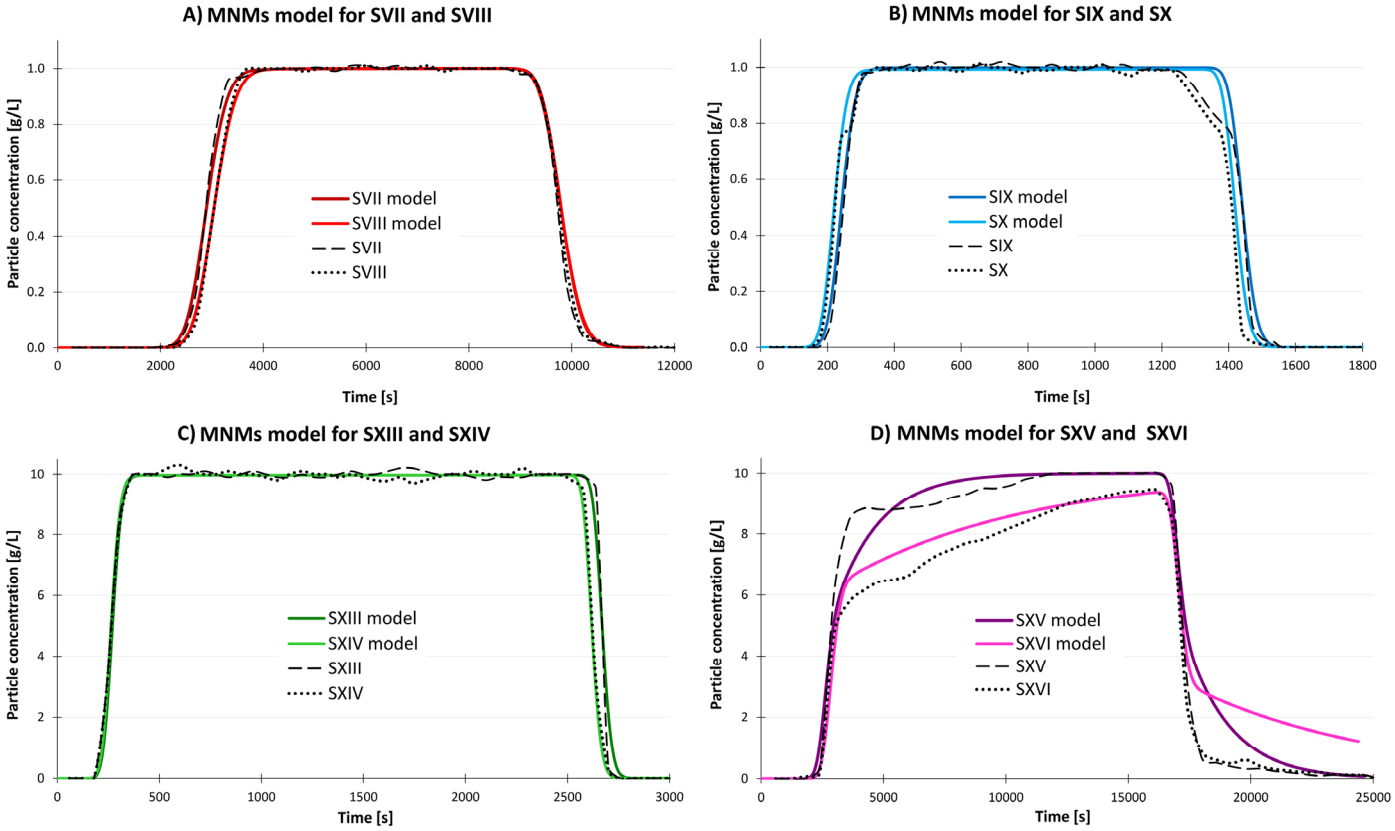

Figure 4.8: Breakthrough curves of particle concentration as a function of time (the output of the MNMs software) of the four column experiments (A: SVII and SVIII, B: SIX and SX, C: SXIII and SXIV, D: SXV and SXVI) (total iron values) as dashed and dotted lines, and their modeled and fitted breakthrough curves as continuous colored lines.

The poorest match between modeled and measured values was observed for the columns SXV and SXVI (D in Figure 4.8), where also the greatest difference between the two columns themselves was seen. The unusual drop of total iron during the flushing of the columns SIX and SX in B already discussed in 4.3.1 was not possible to model, leaving the riddle further unsolved.

4.4.2 Transport parameters

The actual results from the models, the transport parameters (k_a and k_d), are listed in Table 4.4. To get an idea of the mobility of the particles the ratio k_d/k_a is given; the bigger the ratio, the more mobile the particles. Playing the part of a reference for the 2nd GNPs, the transport parameters of all the 1st GNPs column experiments are given as one mean value. The transport parameters for the 2nd GNPs are given as a mean value for each duplicate. For better comparison, also the transport parameters for the columns SXI and SXII are given, although they were not discussed in detail earlier.

Table 4.4: Transport parameters k_a (attachment coefficient) and k_d (detachment coefficient), and k_d/k_a as results from the column models (mean values), listed according to batch of GNPs, particle concentration and flow rate (fast = 10.5 mL/min, slow = 1.06 mL/min) used in the modeled experiments.

	Columns	k_a [1/s]	k_d [1/s]	k_d/k_a
1st GNPs all	SI - SVIII	5.59×10^{-5}	1.10×10^{-3}	19.7
2nd GNPs fast 1g/L	SIX - SX	2.16×10^{-5}	1.00×10^{-4}	4.6
2nd GNPs fast 10g/L	SXIII - SXIV	1.40×10^{-5}	1.00×10^{-4}	7.1
2nd GNPs slow 1g/L	SXI - SXII	3.77×10^{-4}	4.44×10^{-4}	1.2
2nd GNPs slow 10g/L	SXV - SXVI	2.22×10^{-4}	4.79×10^{-4}	2.2

The 1st GNPs were with a k_d/k_a ratio of 19.7 unmistakably more mobile than the 2nd GNPs with an overall k_d/k_a ratio of 1.8. However, this was to expect, since the 1st GNPs have a more negative zeta potential, and a 3 fold amount of TOC (HSs to stabilize the particles) compared to the 2nd GNPs. Also the fact that the lower concentrated GNP

suspensions (1 g/L) showed higher k_d/k_a ratios (an average of 1.4) than the higher concentrated ones (10 g/L, with an average of 2.5) was predictable, considering the effect of concentration (see 4.2.4).

4.4.3 Effect of flow rate on iron oxide NPs mobility

The flow rate seems to have quite an impact on the particle mobility. GNPs transported with a flow rate of 10.5 mL/min through the column showed higher k_d/k_a ratios (an average of 5.61) than particles transported with only 1.06 mL/min (an average k_d/k_a ratio of 1.54). This can be associated to the fact that hydrodynamic drag mitigates deposition and promotes re-entrainment of colloids under unfavorable deposition conditions (e.g. the presence of repulsive energy barriers regarding DLVO theory). This effect results in decreasing attachment rates and increasing detachment rates resulting in increasing k_d/k_a ratios with increasing flow rates (Li et al., 2005; Tong & Johnson, 2006; Tosco et al., 2012). Additionally this effect gets strongly amplified by the higher particle concentration, where the k_d/k_a ratio increases from 4.6 to 7.1.

4.5 Detection of iron oxide NPs in the container experiment - pilot scale

4.5.1 Hydraulic model

The particle tracking was performed using PMPATH to visualize the flow paths within the hydraulic model, representing the real container. The delivered flow paths were to be expected, considering the distribution of the two sand types within the container (see Figure 4.9).

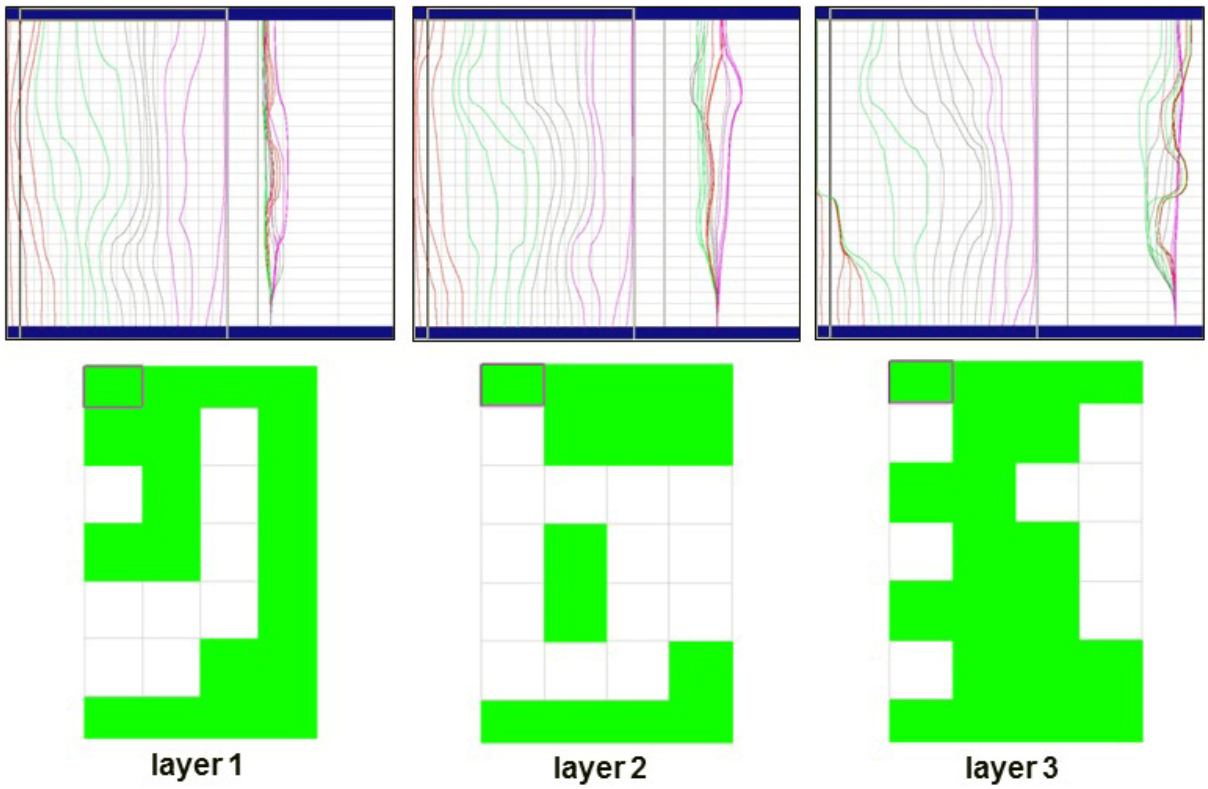

Figure 4.9: Flow paths through the container in the three different layers (groundwater flows from the bottom to the top of the images). The left sides of the flow path images show the container from above, the right sides show the container from the orographic right side. The distribution of the cuboids of the two different sand types in the three layers are shown for a better understanding of the flow paths.

The output of the particle tracking, including the injection well, is shown in Figure 4.10. As expected, modelled flow paths were in accordance with the distribution of the cuboids.

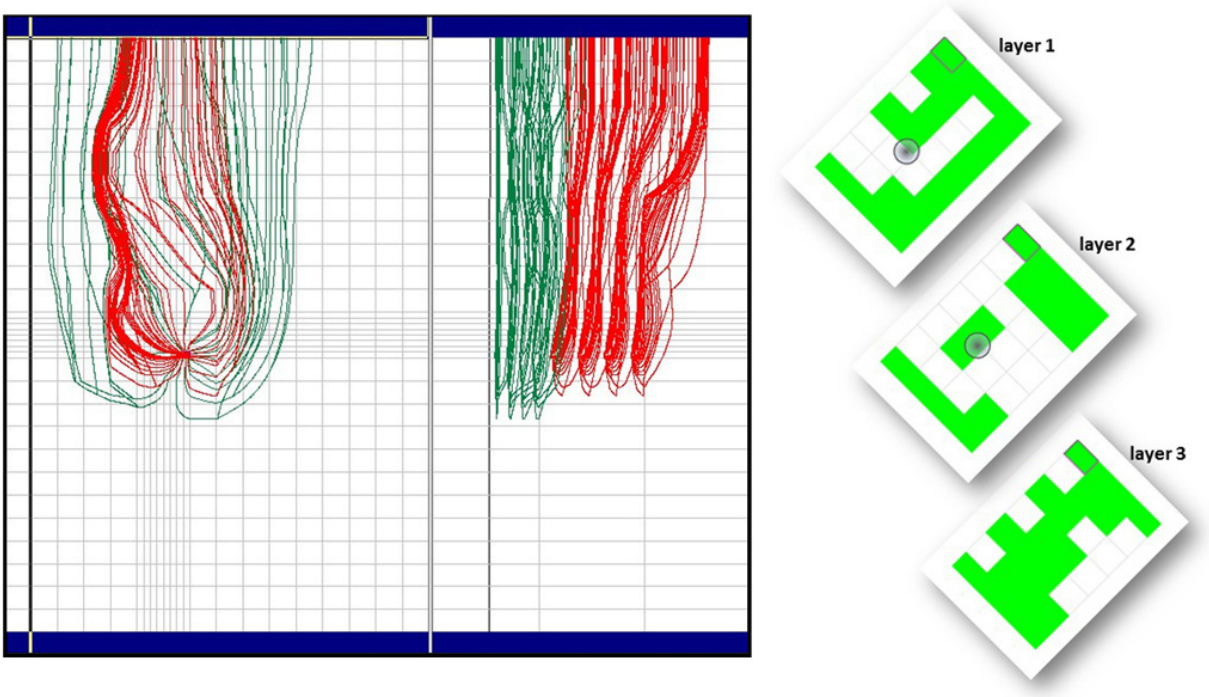

Figure 4.10: Flow paths of hypothetical particles (HPs) placed within the injection well. In green: flow paths of HPs injected in layer 1. In red: flow paths of HPs injected in layer 2. The left side of the flow path image shows the container from above, right side shows the container from the orographic right side (groundwater flows from the bottom to the top of the image). The distribution of the cuboids of the two different sand types in the three layers are shown for a better understanding of the flow paths.

4.5.2 Sampling plan

The results from the hydraulic model (particle tracking) were combined with the mobility parameters of the GNPs (attachment and detachment rates), derived from the column experiments, to develop a sampling plan. The sampling strategy included taking samples from 48 points distributed in the anticipated spreading area of the GNP suspension in layer 1 and 2. One set of samples were taken before the injection (see Figure 4.11). After the start of the injection, samples were taken every 30 minutes for eight hours, then again once after 12, 24, and 48 hours, adding up to a total of 912 samples. If something would have present itself differently during the sampling campaign than anticipated, the sampling plan was open for changes.

Figure 4.11: Photo of the upper half of the container at VEGAS, with the sampling ports (with tubes connected to them) on the side wall. The other part of the container and its sampling ports are accessible from the lower level of the facility. On top are the full tanks with the GNP suspension.

4.5.3 Data from the container experiment

As already mentioned in 2, the data from the container experiment will not be discussed in detail in this thesis, although a short overview is given.

The GNP suspension for the container experiment was prepared on site with a supposed particle concentration of 10 g/L. However, after examining the prepared GNP suspension with the methods approved in batch and lab scale, the particle concentration was determined to be 6.97 ±0.85 g/L. This GNP suspension appeared to contain 230.8 ±84.2 mg/L total iron (translating to 367.2 ±134.0 mg/L goethite), and had a turbidity of 7117 ±184 NTU.

Subsequently the measured samples from 10 of the overall 48 sampling points (sampled 15 times over 25 hours) close to the injection well are presented:

- level 2, row d , columns C and D (**2dC** and **2dD**)
- level 2, row e, columns C, D, and E (**2eC**, **2eD**, and **2eE**)
- level 3, row d, columns C and D (**3dC** and **3dD**)
- level 3, row e, columns C, D, and E (**3eC**, **3eD**, and **3eE**)

The location of the sampling points is shown in Figure 4.12.

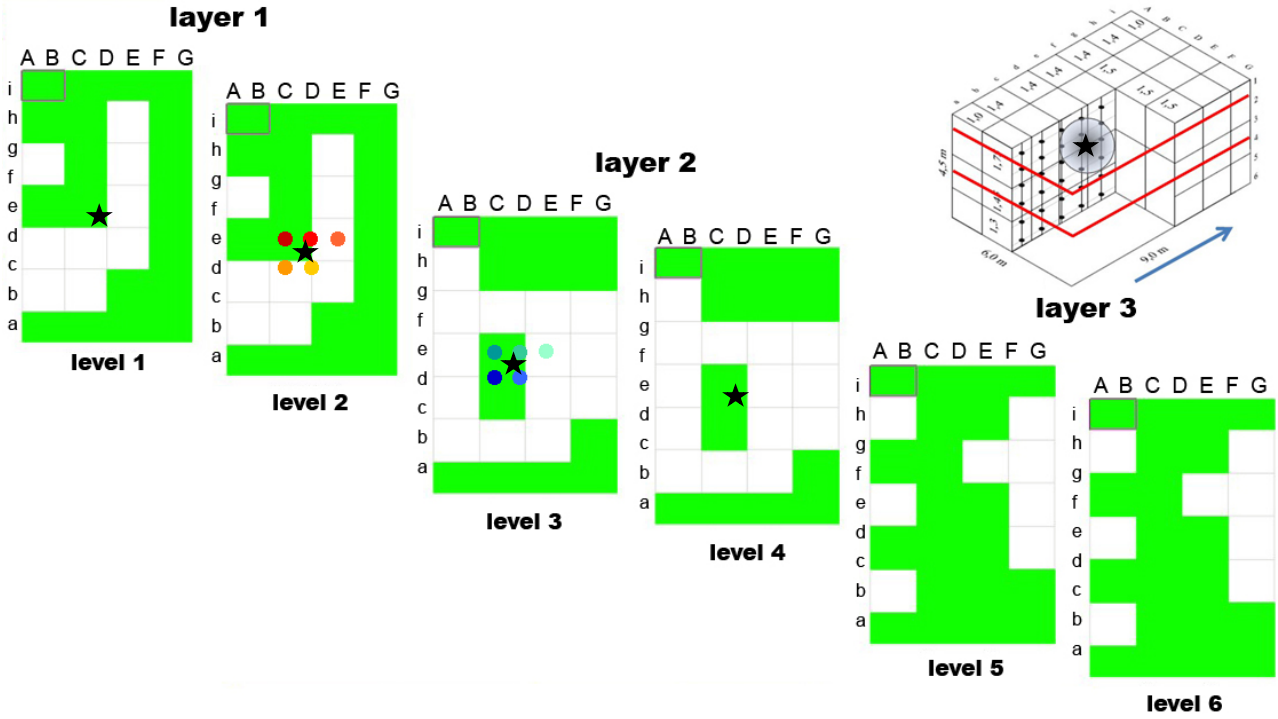

Figure 4.12: The position of the 10 sampling points within the VEGAS container in level 2 and 3 near the injection well (black star). The white and green blocks show the distribution of the two types of M.II, the small figure of the container in the upper right corner is for better orientation of the layers and levels (for more detail see Figure 3.6).

4.5.3.1 Total iron - pilot scale

The fractional concentration of total iron (C/C_0) of the samples over time is shown in Figure 4.13. The presented data show that GNP suspension first reached the sampling points nearest to the injection well, traveled faster in the coarse sand than in the medium sand, and did not travel faster downstream than upstream, at least not that

close to the injection well. Even though the GNP suspension did not travel faster up- than downstream, the C/C_0 is certainly higher for sampling points upstream (row e) from the injection well, than downstream (row d). Further it can be seen that the suspension was washed quite fast from the vicinity of the sampling points in the coarse sand, after injection stopped (after 8 h and 45 min). Near the sampling points in the medium sand there was, after injection stopped, an initial fast decline in total iron concentration which later developed to a stable and very slow decline. The total iron data was not unexpected, with the exception of the extremely high total iron concentrations between 1 and 8 g/L (4 to 35 times the GNP suspension concentration), or even up to 149 g/L (650 times the GNP suspension concentration) in 3dC. An explanation could be that there were already high amounts of iron in the system (sand or tubes) which got mobilized by the GNP solution and/or the heightened flow rate due to the injection. Before the injection started, no iron coming from the sampling points was measured.

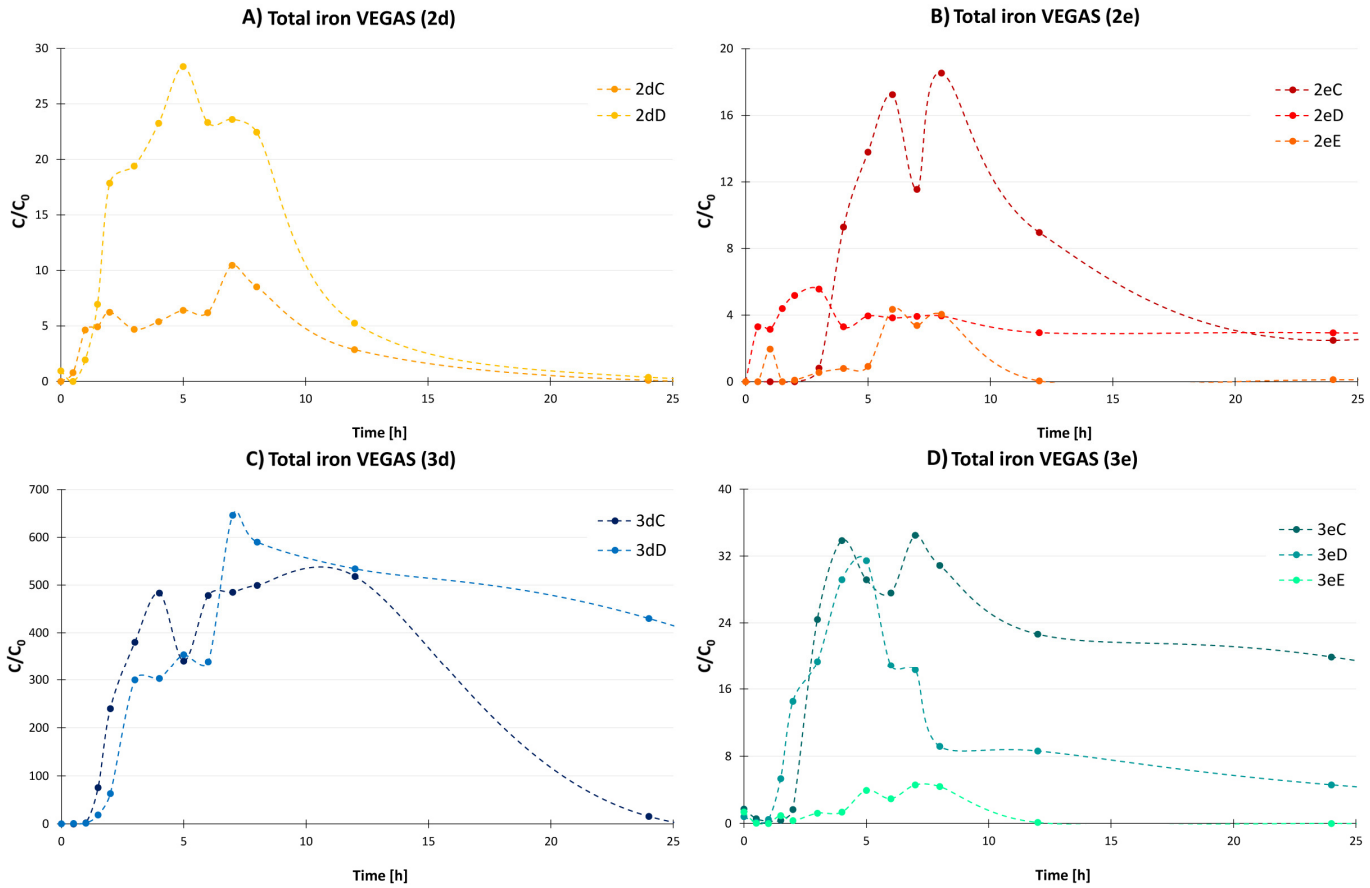

Figure 4.13: Total iron (C/C_0) at the 10 sampling points in layer 2 and 3 over time, near the injection well. The colored dashed lines are plotted to guide the readers' eyes, without suggesting exact trends.

4.5.3.2 Turbidity - pilot scale

The fractional turbidities (C/C_0) of the samples from the 10 sampling points showed almost identical breakthroughs to the total iron (see Figure 4.14). Except that the turbidity values were, unlike the iron values, within the expected range. The sampling points 2eE and 3eE were both reached by extremely (2eE) or strongly diluted GNP suspension (3eE). The turbidity values were, in the beginning, higher (1.2 to 1.6 times the GNP suspension turbidity) than the 7117 NTU of the injected GNP suspension, but as seen in the column experiments, this can be accredited to background turbidity flushed out by the GNP suspension (higher density or mobilization due to HSs). As well as for the total iron also for the turbidity, the C/C_0 values were higher upstream (row d) the injection well than downstream (row e). Further this discrepancy was more distinct in level 2 than 3. This difference can be explained by considering the distribution of the cuboids with the two different sand types, and with the fact that most of the suspension flow happened in the coarse sand rather than in the medium sand.

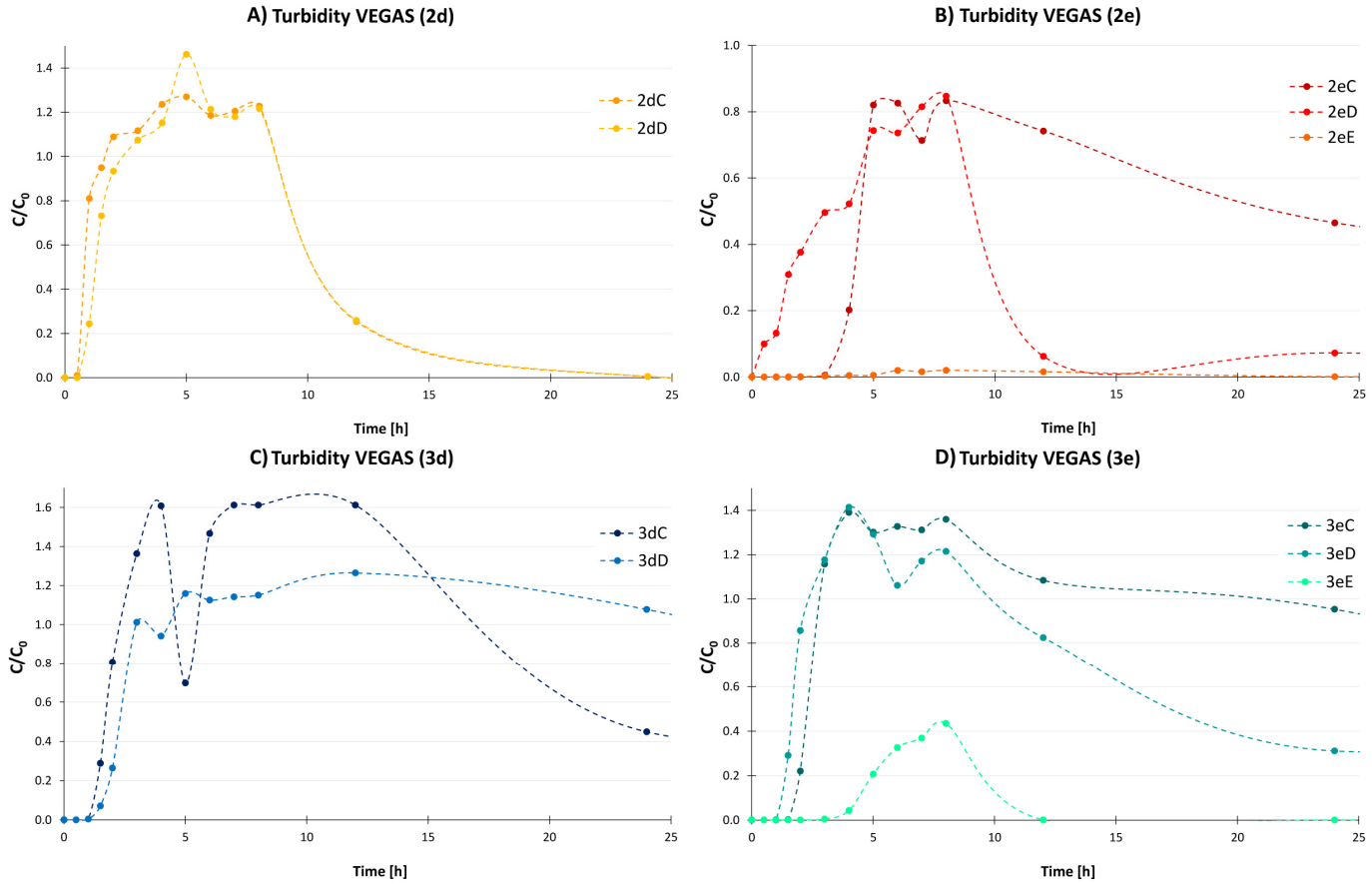

Figure 4.14: Turbidity (C/C_0) at the 10 sampling points in layer 2 and 3 over time, near the injection well. The dashed lines are merely for clarity, and don't suggest exact trends.

4.5.3.3 Turbidity vs total iron - pilot scale

To see how the turbidity data fit to the total iron data they were plotted against each other (see Figure 4.15). From the plot a general trend can be seen, but with a coefficient of determination of merely $R^2 = 0.71$ this is far from a good consensus. After seeing the well matching total iron and turbidity breakthrough curves this might come as a surprise. However, considering that the total iron values are 4 to 650 times the injected GNP suspension, in combination with the 1.2 to 1.6 fold turbidity of the injected GNP suspension, this is comprehensible.

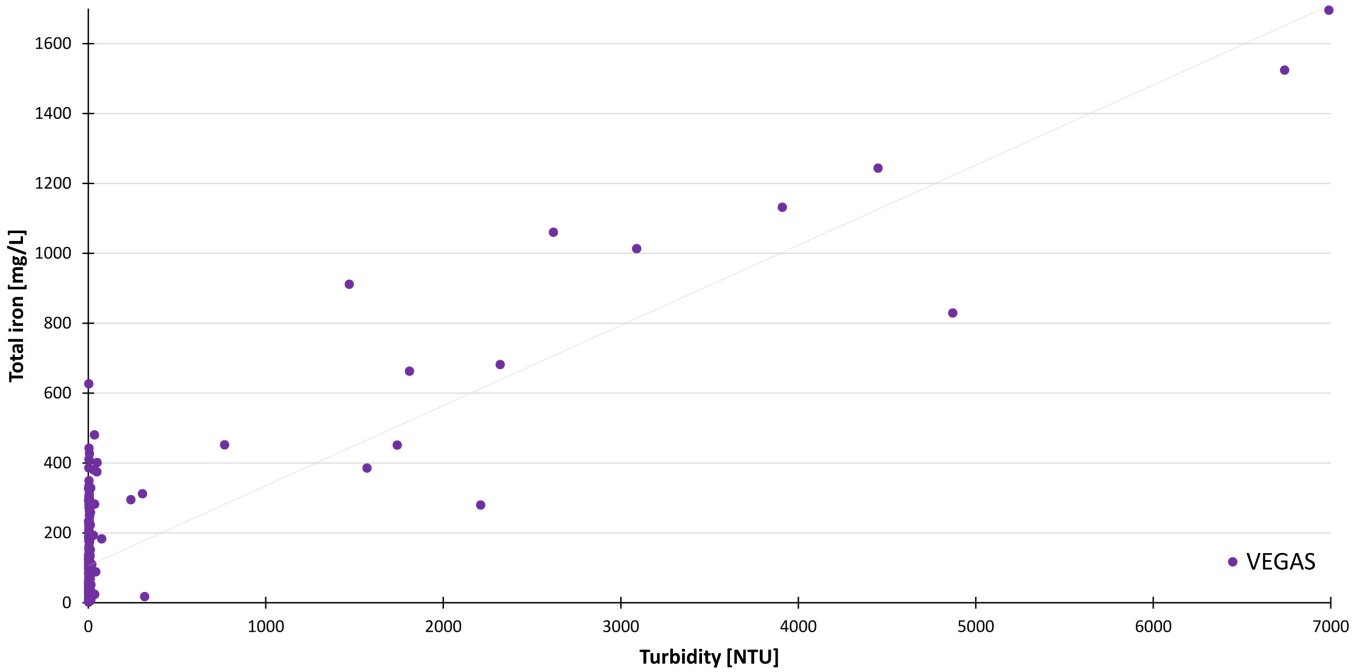

Figure 4.15: Turbidity against the total iron data from the VEGAS container experiment. Trend line in light gray.

4.5.3.4 Particle size - pilot scale

The change of particle size over time during the container experiment (see Figure 4.16) was very similar to the lab scale column experiments, even though the scales were quite different. In the beginning particle sizes between 400 nm and 1 µm were measured, but since neither total iron nor turbidity were measured that early, it can be

assumed that these values belong to something suspended in the container water and not to GNPs. When GNPs (confirmed by total iron and turbidity) were measured, the particle size was somewhere between 400 and 600 nm, like in the column experiments. From there the size further decreased to values between 200 and 300 nm (still agreeing with the column experiments). When the GNP injection stopped, the particle size started to rise again, quite fast in the sampling points within the coarse sand and slowly but steady within the medium sand. Even the arrival of an extremely (2eE) or strongly diluted part of the GNP suspension (3eE) after 5 h could be observed by a slight size change (size data for this sampling point was available only between 4 and 8 h) in both points.

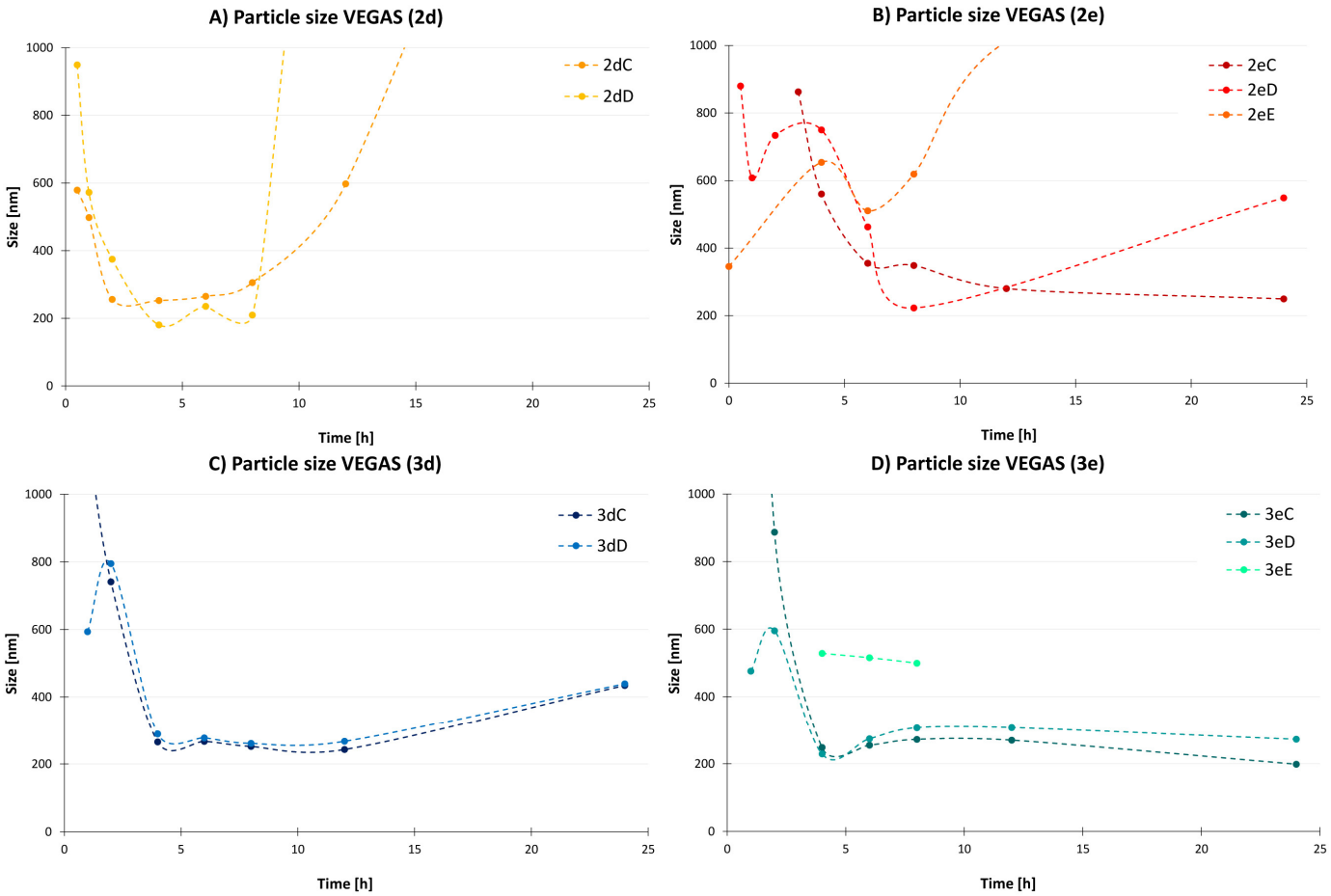

Figure 4.16: The size of the GNPs as a function of time at the 10 sampling points in layer 2 and 3. The colored dashed lines are plotted to guide the readers' eyes, without suggesting exact trends.

5 Conclusions and Outlook

The 2nd GNPs for which the detection methods were tested for, were characterized to have a hydrodynamic particle size of 228 nm, a zeta potential of -22 mV, contain 64 mg/L total iron or 101 mg/L goethite, and 73 mg/L TOC (as HSs), and exhibited a turbidity of 940 NTU in a 1 g/L (particle concentration) dilution in the F.I.m used for most experiments.

From the tested methods of particle detection, only DLS (particle size), 90° scatter method (turbidity of the GNP suspensions), and ICP-OES (total iron concentrations), proved to be suitable for all three scales of the experiments. In addition to particle detection, turbidity measurements can also be used to calculate the particle concentration of the measured suspension.

While testing the methods on the 2nd GNPs several properties that affect aggregation, size, sedimentation, zeta potential, and mobility of the particles were found: The ionic strength of water, which the particles came in contact with, lead to double layer compression, resulting in a drop of zeta potential towards more positive values, and an increase in particle size. At a pH of ~7.8 the PZC for iron oxide NPs was reached, causing aggregation and sedimentation of the particles. Also the particle concentration in the suspension affected the particle size. Finally, the flow rate with which the particles got transported through the porous medium was found to have an influence on deposition and re-entrainment of the particles onto or from this medium (regarding DLVO theory).

Additionally to testing the detection methods, the column experiments were conducted to get an insight of the 2nd GNPs mobility. By modeling the data from the column experiments, transport parameters were derived. Compiling the mass balance of the 2nd GNPs in the column experiments allowed to calculate the rate of particles which got recovered at the outflow of the columns compared to the particles injected (recovery rate). A recovery rate of 0.98 showed that the 2nd GNPs are highly mobile; the same could also be seen from the shape of the breakthrough curves of both total

iron and turbidity. Only if 2nd GNP suspensions with high particle concentrations (10 g/L) were injected in combination with a low flow rate (of 1.06 mL/min corresponding to a flow velocity of 10 m/d), particles got retained within the porous medium, reducing the recovery rate down to a minimum of 0.72. This retention of the particles could be seen from the shape of the breakthrough curves, too. The models of the column experiments delivered very similar results only expressed in attachment (k_a) and detachment (k_d) rates. Using the k_d/k_a ratio showed that the flow rate had the biggest influence on NP mobility. The particles were 3 times more mobile if pumped with a flow rate of 10.5 mL/min instead of 1.06 mL/min. A travel distance according to Laumann et al. (2013) or Tosco et al. (2012) could not be calculated since the used porous medium was a heterogeneous sand (M.II) and not a homogenous standard sand as required for such calculations.

All the data, measured and modeled, in batch and lab scale experiments, were used to carry out a successful sampling campaign at the pilot scale experiment at VEGAS. The data collected at the VEGAS experiment was not discussed in detail in this thesis, but some selected sampling points were shown, to demonstrate the effectivity, but also the limits of the measured parameters which are susceptible to errors. Total iron measurements were influenced by iron present in the container and mobilized by the NP injection. Turbidity values were in the beginning of the injection slightly increased by background turbidity, also mobilized by the NP injection. The particle size delivered excellent results, though. However, by comparing the results of total iron, turbidity, and particle size of the samples with each other, and to the injected NP suspension, it is possible to identify these errors and to correct them.

The results of this thesis and the pilot scale experiment will be used in a designated field test, where the iron oxide NPs will be injected into a contaminated aquifer body in the Czech Republic.

6 Acknowledgements

At this point I would like to express my gratitude:

Towards Prof. Dr. Thilo Hofmann as supervisor of my thesis.

Towards Dr. Stephan Wagner and Dr. Milica Velimirovic for introducing me to the topic of this thesis, long discussions, helpful feedback, inspiration, and their positive attitude.

Towards MSc. Doris Schmid for taking me under her wing regarding the work in the laboratory, sharing her expertise, and helpful advice.

Towards my fellow students and friends for helpful chats in the laboratory and cheerful lunch breaks.

And most importantly towards my parents, grandparents, and Conny for unconditional support in my studies.

7 Bibliography

Akamatsu, K. & Deki, S. (1997). Nanoscale metal particles dispersed in polymer matrix. NanoStructured Materials, 8 (8), 1121-1129.

Baalousha, M. (2009). Aggregation and disaggregation of iron oxide nanoparticles: Influence of particle concentration, pH and natural organic matter. Science of the Total Environment, 407, 2093-2101.

Bardos, P., Bone, B., Daly, P., Elliott, D., Jones, S., Lowry, E. & Merly, C. (2014). A Risk/Benefit Appraisal for the Application of Nano-Scale Zero Valent Iron (nZVI) for the Remediation of Contaminated Sites (Supporting MS3 - NanoRem information for decision makers – initial version). Available from www.nanorem.eu/Displaynews.aspx?ID=525 [25.03.2015].

Bennett, P., He, F., Zhao, D., Aiken, B. & Feldman, L. (2010). In situ testing of metallic iron nanoparticle mobility and reactivity in a shallow granular aquifer. Journal of Contaminant Hydrology, 116, 35-46.

Bosch, J., Fritzsche, A., Totsche, K.U. & Meckenstock, R.U. (2010)a. Nanosized Ferrihydrite Colloids Facilitate Microbial Iron Reduction under Flow Conditions. Geomicrobiology Journal, 27 (2), 123-129.

Bosch, J., Heister, K., Hofmann, T. & Meckenstock R.U. (2010)b. Nanosized Iron Oxide Colloids Strongly Enhance Microbial Iron Reduction. Appl. Environ. Microbiol., 76 (1), 184-189.

Braunschweig, J., Bosc,h J. & Meckenstock R.U. (2013). Iron oxide nanoparticles in geomicrobiology: from biogeochemistry to bioremediation. New Biotechnology, 30 (6), 793-802.

Christiansen,C.M., Damgaard, i., Broholm, M., Kessler, T., Klint, K.E., Nilsson, B. & Bjerg, P.L. (2010). Comparison of Delivery Methods for Enhanced In situ Remediation in Clay Till. Ground Water Monitoring & Remediation, 30 (4), 107-122.

Chrzanowska N. & Załeska-Radziwiłł, M. (2014). The impacts of aluminum and zirconium nano-oxides on planktonic and biofilm bacteria. Desalination and Water Treatment, 52 (19-21), 3680-3689.

Crane, R.A. & Scott, T.B. (2012). Nanoscale zero-valent iron: Future prospects for an emerging water treatment technology. Journal of Hazardous Materials, 211/212, 112-125.

Cundy, A.B., Hopkinson, L. & Whitby, R.L.D. (2008). Use of iron-based technologies in contaminated land and groundwater remediation: A review. Science of the total environment, 400, 42-51.

De Boer C.V. (2012). Transport of Nano Sized Zero Valent Iron Colloids during Injection into the Subsurface. Mitteilungen Institut für Wasser- und Umweltsystemmodellierung, Universität Stuttgart, 215.

Delgado, A.V., González-Caballero, F., Hunter, R.J., Koopal, L.K. & Lyklema, J. (2005). Measurement and Interpretation of Electrokinetic Phenomena (IUPAC Technical Report). Pure Appl. Chem., 77 (10), 1753-1805.

Dong, Y., Gandhi, N. & Hauschild, M.Z. (2014). Development of Comparative Toxicity Potentials of 14 cationic metals in freshwater. Chemosphere, 112, 26-33.

Elimelech, M., Gregory, J., Jia, X. & Williams, R. A. (1995). Particle Deposition and Aggregation: Measurement, Modelling and Simulation. Butterworth-Heinemann.

Elimelech, M., Nagai, M., Ko, C.C. & Ryan, J.N. (2000). Relative Insignificance of Mineral Grain Zeta Potential to Colloid Transport in Geochemically Heterogeneous Porous Media. Environ. Sci. Technol., 34, 2143-2148.

Elliott, D.W. & Zhang, W.X. (2001). Field Assessment of Nanoscale Bimetallic Particles for Groundwater Treatment. Environ. Sci. Technol., 35, 4922-4926.

Fu, F., Dionysiou, D.D. & Liu, H. (2014). The use of zero-valent iron for groundwater remediation and wastewater treatment: A review. Journal of Hazardous Materials, 28, 194-205.

Geiger, C.L., Carvalho-Knighton, K., Novaes-Card, S., Maloney, P. & DeVor, R. (2009). A Review of Environmental Applications of Nanoscale and Microscale Reactive Metal Particles. ACS Symposium Series; American Chemical Society: Washington, DC.

Gregory, J. (2004). Particles in water: properties and processes. IWA Publishing.

Grillo, R., Rosa, A.H. & Fraceto, L.F. (2015). Engineered nanoparticles and organic matter: A review of the state-of-the-art. Chemosphere, 119, 608-619.

Henn, K.W. & Waddill, D.W. (2006). Utilization of nanoscale zero-valent iron for source remediation - A case study. Remediation Journal, 16 (2), 57-77.

Hosseini, S.M. & Tosco, T. (2013). Transport and retention of high concentrated nano-Fe/Cu particles through highly flow-rated packed sand column. Water research, 47, 326-338.

Jaisi, D.P., Saleh, N.B., Blake, R.E. & Elimelech, M. (2008). Transport of single-walled carbon nanotubes in porous media, filtration mechanisms and reversibility. Environmental Science & Technology, 4222, 8317-8323.

Johnson, R.L., Johnson, G.O., Nurmi, J.T. & Tratnyek, P.G. (2009). Natural organic matter enhanced mobility of nano zerovalent iron. Environ. Sci. Technol., 43, 5455-5460.

Johnson, R.L., Nurmi, J.T., O'Brien Johnson, G.S., Fan, D., O'Brien Johnson, R.L., Shi, Z., Salter-Blanc, A.J., Tratnyek, P.G. & Lowry, G.V. (2013). Field-Scale Transport and Transformation of Carboxymethylcellulose-Stabilized Nano Zero-Valent Iron. Environ. Sci. Technol., 47, 1573-1580.

Kanel, S.R., Nepal, D., Manning, B. and Choi, H. (2007). Transport of surface-modified iron nanoparticle in porous media and application to arsenic(III) remediation. Journal of Nanoparticle Research, 9 (5), 725-735.

Kango, S., Kalia, S., Celli, A., Njuguna, J., Habibi, Y. & Kumar, R. (2013). Surface modification of inorganic nanoparticles for development of organic-inorganic nanocomposites - A review. Progress in Polymer Science, 38, 1232-1261.

Kaszubas, M., Corbett, J., McNeil Watson, F. & Jones, A. (2010). High-concentration zeta potential measurements using light-scattering techniques. Phil. Trans. R. Soc. A, 368, 4439-4451.

Kato, H., Nakamura, A., Takahashi, K. & Kinugasa, S. (2012). Accurate Size and Size-Distribution Determination of Polystyrene Latex Nanoparticles in Aqueous Medium Using Dynamic Light Scattering and Asymmetrical Flow Field Flow Fractionation with Multi-Angle Light Scattering. Nanomaterials, 2, 15-30.

Kretzschmar, R., Borkovec, M., Grolimund, D. & Elimelech, M. (1999). Mobile subsurface colloids and their role in contaminant transport. Adv. Agron., 66, 121-193.

Lauman, S., Micic, V., Lowry, G.V. & Hofmann, T. (2013). Carbonate minerals in porous media decrease mobility of polyacrylic acid modified zero-valent iron nanoparticles used for groundwater remediation. Environmental Pollution, 179, 53-60.

Lewis, J. & Sjöstrom, J. (2010). Optimizing the experimental design of soil columns in saturated and unsaturated transport experiments. Journal of Contaminant Hydrology, 115, 1-13.

Li, X., Zhang, P., Lin, C.L. & Johnson, W.P. (2005). Role of Hydrodynamic Drag on Microsphere Deposition and Re-entrainment in Porous Media under Unfavorable Conditions. Environ. Sci. Technol., 39, 4012-4020.

Lowery, G.V., Gregory, K.B., Apte, S.C. & Lead, J.R. (2012). Transformations of Nanomaterials in the Environment. Environ. Sci. Technol., 46 (13), 6893-6899.

Lowery, G.V. & Johnson, M. (2004). Congener-Specific Dechlorination of Dissolved PCBs by Microscale and Nanoscale Zerovalent Iron in a Water/Methanol Solution. Environ. Sci. Technol., 38, 5208-5216.

Maurer-Jones, M.A., Gunsolus, I.L., Murphy, C.J. & Haynes, C.L. (2013). Toxicity of engineered nanoparticles in the environment. Anal. Chem., 85, 3036-3049.

Maximova, N. & Dahl, O. (2006). Environmental implications of aggregation phenomena: Current understanding. Current Opinion in Colloid & Interface Science, 11, 246-266.

Nurmi, J.T., Tratnyek, P.G., Sarathy, V., Baer, D.B., Amonette, J.E., Pecher, K., Wang, C., Penn, R.L. & Driessen, M.D. (2005). Characterization and Properties of Metallic Iron Nanoparticles: Spectroscopy, Electrochemistry, and Kinetics. Environ. Sci. Technol., 39, 1221-1230.

O'Carroll, D., Sleep, B., Krol, M., Boparai, H. & Kocur, C. (2013). Nanoscale zero valent iron and bimetallic particles for contaminated site remediation. Advances in Water Resources, 51, 104-122.

Phenrat, T., Kim, H.J., Fagerlund, F., Illangasekare, T., Tilton, R.D. & Lowry, G.V. (2009). Particle size distribution, concentration, and magnetic attraction affect transport of polymer- modified Fe^0 nanoparticles in sand columns. Environmental Science & Technology, 43, 5079-5085.

Saleh, N., Kim, H.-J., Phenrat, T., Matyjaszewski, K., Tilton, R.D. & Lowry, G.V. (2008). Ionic strength and composition affect the mobility of surface-modified Fe0 nanoparticles in water saturated sand columns. Environmental Science & Technology, 42 (9), 3349-3355.

Shih Y. & Tai, Y. (2010). Reaction of decabrominated diphenyl ether by zerovalent iron nanoparticles. Chemosphere, 78, 1200-1206.

Simonet, B.M. & Valcárcel, M. (2009). Monitoring nanoparticles in the environment. Anal. Bioanal. Chem., 393, 17-21.

Stephens, D.B., Hsu, K-C., Prieksat, M.A., Ankeny, M.A., Blandford, N., Roth, T.L., Kelsey, J.A. & Whitworth, J.R. (1998). A comparison of estimated and calculated effective porosity. Hydrogeology Journal, 6, 156-165.

Swartjes, F.A. (2011). Introduction to contaminated site management. In Swartjes, F.A. (editor), Dealing with Contaminated Sites (3-89). Netherlands: Springer.

Szalai, Z., Kiss, K., Jakab, G., Sipos, P., Belucz, B. & Németh, T. (2013). The use of UV-VIS- NIR reflectance spectroscopy to identify iron minerals. Astron. Nachr., 334 (9), 940-943.

Tong, M. & Johnson, W.P. (2006). Excess Colloid Retention in Porous Media as a Function of Colloid Size, Fluid Velocity, and Grain Angularity. Environ. Sci. Technol., 40, 7725-7731.

Tosco, T. & Sethi, R. (2009). MNM1D: A Numerical Code for Colloid Transport in Porous Media: Implementation and Validation. American Journal of Environmental Sciences, 5 (4), 217-525.

Tosco, T. & Sethi, R. (2010). Transport of Non-Newtonian Suspensions of Highly Concentrated Micro- And Nanoscale Iron Particles in Porous Media: A Modeling Approach. Environ. Sci. Technol., 44, 9062-9068.

Tosco, T., Bosch, J., Meckenstock, R.U. & Sethi, R. (2012). Transport of Ferrihydrite Nanoparticles in Saturated Porous Media: Role of Ionic Strength and Flow Rate. Environmental Science & Technology, 46, 4008-4015.

Tosco, T., Petrangeli Papini, M., Cruz Viggi, C. & Sethi, R. (2014). Nanoscale zerovalent iron particles for groundwater remediation: a review. Journal of Cleaner Production, 77, 10-21.

Tratnyek, T.G. & Johnson, R.L. (2006). Nanotechnologies for environmental cleanup. Nanotoday, 1 (2), 44-48.

Tufenkji, N. & Elimelech, M. (2004). Deviation from the classical colloid filtration theory in the presence of repulsive DLVO interactions. Langmuir 20, 10818-10828.

US EPA, (2002). Methods for measuring the acute ecotoxicity of efluents and receving waters to freshwater and marine organisms. Fifth edition. EPA-821-R-02-012. Available from www.epa.gov [13.04.2015].

US EPA, (2006). Voluntary Estuary Monitoring Manual, A Methods Manual, Second Edition, EPA-842-B-06-003. Chapter 15: Turbidity and Total Solids. Available from www.epa.gov [23.03.2015].

Van der Zee, C., Roberts, D.R., Rancourt, D.G. & Slomp, C.P. (2003). Nanogoethite is the dominant reactive oxyhydroxide phase in lake and marine sediments. Geology, 31 (11), 993-996.

Wang, R.K., Chen, W.C., Campos, D.K. & Ziegler, K.J. (2008). Swelling the micelle core surrounding single-walled carbon nanotubes with water-immiscible organic solvents. Journal of the American Chemical Society, 130, 16330-16337.

Waychunas, G.A., Kim, C.S. & Banfield, J.F. (2005). Nanoparticulate iron oxide minerals in soils and sediments: unique properties and contaminant scavenging mechanisms. Journal of Nanoparticle Research, 7, 409-433.

Weber, K.A., Achenbach, L.A. & Coates J.D. (2006). Microorganisms pumping iron: anaerobic microbial iron oxidation and reduction. Nat. Rev. Microbiol., 4, 752-764.

8 Appendix

8.1 Statutory Declaration

I declare that I have authored this thesis independently, that I have not used other than the declared sources/resources, and that I have explicitly marked all material which has been quoted either literally or by content from the used sources.

Vienna, _____ _____
Date Signature

8.2 Eidesstattliche Erklärung

Ich erkläre an Eides statt, dass ich die vorliegende Arbeit selbstständig verfasst, andere als die angegebenen Quellen/Hilfsmittel nicht benutzt, und die den benutzten Quellen wörtlich und inhaltlich entnommenen Stellen als solche kenntlich gemacht habe.

Wien, am _____ _____
Datum Unterschrift

8.3 Curriculum Vitae

Contact information

Name	Stefan Holzner
Address	Andreasgasse 5/1/4, A-1070 Vienna
Telephone	+43 650 4212087
E-mail	holznerstefan@hotmail.com

Personal information

Date of birth	January 30th, 1984
Place of birth	Meran/Merano
Citizenship	Italian (South Tyrol)

Education

10/2012 - present	M.Sc. Environmental Sciences *University of Vienna* Master Thesis: Monitoring techniques for studying mobility of iron oxide nanoparticles during field application Supervisor: Univ.-Prof. Dr. Thilo Hofmann
10/2004 - 08/2011	Mag.Rer.Nat. Geosciences *University of Innsbruck* Diploma Thesis: Geologie des südlichen Fanesgebietes östlich von St Kassian (Südtiroler Dolomiten) unter besonderer Berücksichtigung der Blockgletscher Supervisor: Ao.-Univ.-Prof. Dr. Karl Krainer
10/2003 - 06/2004	Two semesters Chemistry *University of Innsbruck*
09/1998 - 07/2003	Academic high school *Albert Einstein Meran (mathematical and natural sciences)*
09/1990 - 06/1998	Elementary and secondary school in Lana

Work experience

09/2010 - 12/2012	Internship at the TU-Mountain-Academy Freiberg (Faculty 3, Institute for Geology & Remote sensing) Mapping faults in the Kabul and Pamir region (Afghanistan and Tajikistan). Interpretation of satellite-images and laser-scans by means of software like Quantumgis, Envi, Geomatica and TecDem.
2008 - 2010	In the summer and fall months geological mapping and analytical field investigation in the Fanes area in the Dolomites (South Tyrol) for the diploma thesis.

07/2007 - 09/2007	Collaboration in the “Bureau for Geology and Environment Dr. Konrad Messner”.
1998 - 2006	Seasonal work (summer job) in agriculture (apple- and viticulture)

Skills

Language	*German (mother language)* *English (fluent, TOEFL-iBT: 107 from 120 points)* *Italian (fluent)* *French (basic knowledge)* *Latin (reading/writing)*
Software	*Adobe Photoshop, Adobe Lightroom, ArcGis, AutoCAD, Envi, Geomatica, Microsoft Office, MNM’s, Modflow, Open Office, PhreeqC, Quantum Gis, Stanmod, TecDem, TectonicsFP;* *Operating systems: Microsoft Windows, Mac, and Linux.*

Further activities

Geological excursions

2009	East-Germany (Quaternary geology - archeology excursion in Saxony and Thuringia)
2009	South- and North Tyrol (Geology - paleontology excursion in the Dolomites and the Northern Limestone Alps)
2008	North-Greece (Structural geology excursion in the Rhodopes and Dinarides)
2008	Southern Austria (Structural geology excursion in the Carnic Alps)
2007	South Tyrol (Petrology excursion in eastern South Tyrol)
2007	Southern Austria (Petrology excursion in Styria)
2007	Geological mapping (Sediments in the Fassa-Valley in the Dolomites, Italy)
2007	Geological mapping (Metamorphites in the Kauner-Valley, Austria)
2006	Czech Republic (Paleontology excursion in the Prague Basin)
2006	Northwest Italy (Quaternary geology excursion in the area of the Tagliamento River)
2005	Tyrol (Quaternary geology in the Inn- and Ötz-Valley)
2005	Tyrol (Paleontology excursion in the Inn-Valley)
2005	South Italy (Volcano excursion: Mount Vesuvius, Mount Etna, and Aeolian Islands)

Attended conferences

2014 102nd Annual Conference of the College Art Association, Chicago
2011 1st International Workshop on Geoelectrical Monitoring GELMON 2011, of the Austrian Geological Federal Institute, Vienna
2009 Rockslide Days – If mountains start to slide (Institute of Geology and Paleontology University of Innsbruck), Innsbruck
2009 Living and constructing in permafrost regions (Office for geology and building materials testing South Tyrol), Bozen

Foreign travels

2014 Cambodia, Myanmar, and Thailand
2014 USA (California, Connecticut, Illinois, Nevada, New York, Pennsylvania, and Washington, D.C.)
2013 India and Thailand
2011 USA (Florida, Georgia, Maryland, New York, North Carolina, Pennsylvania, South Carolina, Virginia, and Washington, D.C.)

Meditation retreats

2015 5-day Secular Meditation and Study Retreat by Stephen and Martine Batchelor, Scheibbs (Austria)